High Resolution Arctic Ocean and Sea Ice Simulations. Part I: Ocean Model Design and Early Results

Wieslaw Maslowski, A. Rost Parsons, Yuxia Zhang,

and Albert J. Semtner

Department of Oceanography

Naval Postgraduate School

Monterey, California

Submitted to the Journal of Geophysical Research

March 1997

Abstract

A high-resolution ocean general circulation model has been designed and used to study the Arctic Ocean. The grid spacing is 18 km (1/6-degree in rotated coordinates) with 30 levels. The domain contains the central Arctic Ocean (Canadian and Eurasian Basins), Nordic Seas, Canadian Archipelago, and the subpolar North Atlantic. The model is based on the free-surface Parallel Ocean Climate Model (POCM) of Semtner and Chervin and permits an accurate representation of the unsmoothed Arctic Ocean bathymetry. After one year of initialization using annual mean conditions, a 6-year integration forced at the surface with monthly mean T and S and high-frequency 1992 wind forcing was completed. Results are shown for the large-scale and regional-scale circulations. Boundary currents narrower than 100 km are shown to be primary means for distributing properties throughout the Arctic Ocean. Insights are provided on circulations in the northern North Atlantic, the Labrador Sea, and the Nordic Seas, including the Barents Sea. Transports calculated at different sections across currents carrying water between the northern North Atlantic and the Arctic Ocean compare well with earlier estimates based on observations. In particular the model simulates a northward flow of Atlantic Water of about 7 Sv between Iceland and Scotland, and a cold dense overflow of 2.7 Sv southward from Denmark Strait. In Fram Strait the northward flow of water warmer than 0°C in the West Spitsbergen Current is 3.5 Sv, of which only 1.5 Sv continues as a boundary current along the continental slope, with the rest entering the deep Nansen Basin. There is a net total outflow from the Barents Sea of 2.2 Sv, and all this water feeds the flow along the continental slopes. This analysis supports the earlier hypothesis based on observations that the Barents Sea inflow into the Arctic is equally or even more important than the contribution from Fram Strait.

1. Introduction

Both global climate modeling and observations identify the Arctic as a region of amplified response to global climate change, as well as a region of significant influence on global climate. The Arctic Ocean also has been recently given considerable attention regarding such issues as dispersion of nuclear contamination, biological productivity, and navigational forecasts. An important qualitative result from various climate models is their consistency in predicting that the Arctic will experience the largest temperature rise due to an increase of greenhouse gases. Differences in quantitative predictions from those models result in part from differing assumptions about the effects of processes at various spatial and temporal scales controlling heat, salt, and fresh water balances of the Arctic system.

Some studies predict that the Arctic ice will significantly reduce in area and/or volume and possibly disappear in summer as a result of increased greenhouse gases. The sea-ice albedo-temperature feedback is used to explain this. It implies that at warmer temperatures there will be less sea ice in the Arctic, which, in turn, implies that more solar radiation is absorbed (due to decreased albedo), which will result in even warmer temperatures, and so on. The only stabilizing effect (negative feedback) comes from more rapid radiative cooling of the ice surface at warmer temperatures.

Other negative feedbacks might be possible, should the Arctic Ocean and its sea ice be more realistically represented in global climate models. Warmer air temperature may lead to an enhanced hydrological cycle and greater moisture convergence into the Arctic atmosphere with associated increases in precipitation. Melting large amounts of sea ice at the same time, must lead to dramatic increases in the fresh water flux out from the Arctic. The Great Salinity Anomaly (GSA) of the late 1960s and 1970s is a good example of such an anomalous fresh water event. Some effects of the GSA on the dynamics of the Nordic Seas have been described in literature (Dickson et al., 1988; Aagaard et al., 1991; Meincke

et al., 1990; Hakkinen, 1993; Maslowski, 1995). An excess of fresh water present at the surface of the Nordic Seas alters and may even stop convection there (Aagaard and Carmack, 1989), thus strongly affecting the formation of North Atlantic Deep Water (NADW) which controls the global thermohaline circulation. Weakening of the global meridional overturning cell may result in lower poleward heat fluxes. In the extreme case, changing the present conveyor belt circulation to another stable mode of operation (Bryan, 1986) as a result of shutting down the convection in the subpolar North Atlantic, would cut off the supply of heat to the Arctic Ocean via the Gulf Stream-North Atlantic-Norwegian Atlantic Current system. This would provide an important negative feedback to the above scenario of warming in the Arctic possibly even able to reverse the warming trend. In fact some very cold periods in the past are suggested to be the result of a temporary shutdown of the conveyor, an event also known as the halocline catastrophe (Broecker, 1991). Hence temporary warming trend in the increased greenhouse gases scenario, by melting Arctic sea ice could results in shutting down the conveyor and a cooling period, at least in the North Atlantic.

Climate models need a better representation of the most important physical processes taking place in the Arctic Ocean in order to eliminate the uncertainty in predicting the climate system response, particularly in the Arctic region, to both natural and man-made climate variability. In order to achieve these goals, the interactions between the Arctic Ocean circulation, sea-ice cover, atmosphere, and the hydrological cycle need to be well understood. A high resolution model of the Arctic Ocean with sea ice, combined with continued field studies to acquire data for model forcing and validation, can be used to address some of these interactions. Such a model should consist of a state-of-the-art dynamic-thermodynamic sea-ice model coupled to an eddy-resolving three-dimensional ocean model which includes physical processes specific to the Arctic Ocean. Some important dynamical processes which are specific to the Arctic Ocean are downslope mixing of brine-enriched dense shelf waters and deep water formation in the open ocean. These processes occur

locally but their effects are basin-wide; and that has so far posed a major problem for modelers. The Arctic Ocean, with its size and connectedness approaching planetary scale, has been a difficult basin to model with resolution sufficient to include those important processes as well as to represent energetic baroclinic eddies on a scale of the local radius of deformation, which in the Arctic Ocean is of order 5-10 km. However, recent efforts to model the rest of the world ocean at grid sizes approaching the local radius of deformation have paid off handsomely in reproducing the time and length scales of a variety of currents, as confirmed by satellite altimetry (see Semtner (1995) for an overview). Those successes have been facilitated by advances in computer technology and adaptation of ocean models to use it, by new methods to handle complex topography, and finally by better ways of specifying atmospheric forcing. It is time now to apply those techniques to the Arctic Ocean and to move toward greater realism in its simulation.

In this and subsequent papers we describe results from an ongoing modeling study to improve our understanding of the Arctic Ocean/Sea Ice system. Both model resolution and domain are chosen so as to properly include most of the important processes in the Arctic Ocean. The model domain (Figure 1) includes not only the Central Arctic (Canadian and Eurasian Basins) but also the Nordic Seas, Canadian Archipelago, and the subarctic North Atlantic. Adaptation of recently developed ocean general circulation models, taking advantage of the available computational resources, allows the development of a basin-wide Arctic Ocean and sea ice model approaching eddy resolution. The ocean model is a modified free-surface version of the Semtner/Chervin (Semtner, 1995) Parallel Ocean Circulation Model (POCM). The ocean model, the initial and boundary conditions, and the forcing data are summarized in section 2. Results obtained so far already provide new information to facilitate understanding of key dynamical processes in the Arctic. The results are presented and discussed in section 3 and 4, with a summary and conclusions

following in section 5.

2. Ocean Model Description

To study the three dimensional circulation of the Arctic Ocean, the Semtner/Chervin Parallel Ocean Climate Model is used with a free-surface (Semtner, 1974; Semtner and Chervin, 1988; Killworth et al., 1991, and Semtner, 1995). The model assumes hydrostatic balance and makes the Boussinesq approximation. The finite difference scheme uses an Arakawa B-grid (Mesinger and Arakawa, 1976) and integrates the primitive equations in spherical coordinates. To eliminate the convergence of meridians at the North Pole, a model grid was rotated off the pole placing the equator along the meridians 50°W and 130° E, the meridian 0° E along the meridians 140° W and 40° E, and point (0° N, 0° E) at the North Pole.

The model's prognostic variables and equations to solve for them are:

- u and v in horizontal momentum equations

$$\frac{\partial u}{\partial t} + L(u) - fv = -\frac{1}{\rho_o a \cos\varphi}\frac{\partial p}{\partial \lambda} + \frac{\partial}{\partial z}\left(K_M \frac{\partial u}{\partial z}\right) + B_M \nabla_H^4 (u)$$

$$\frac{\partial v}{\partial t} + L(v) + fu = -\frac{1}{\rho_o a}\frac{\partial p}{\partial \varphi} + \frac{\partial}{\partial z}\left(K_M \frac{\partial v}{\partial z}\right) + B_M \nabla_H^4 (v)$$

- pressure (p) in the hydrostatic equation

$$\frac{\partial p}{\partial z} = -\rho g$$

- vertical velocity (w) in the continuity equation

$$\frac{1}{a\cos\varphi}\frac{\partial u}{\partial \lambda} + \frac{1}{a\cos\varphi}\frac{\partial (v\cos\varphi)}{\partial \varphi} + \frac{\partial w}{\partial z} = 0$$

- potential temperature (T) and salinity (S) in advection-diffusion equations

$$\frac{\partial T}{\partial t} + L(T) = \frac{\partial}{\partial z}\left(K_D \frac{\partial T}{\partial z}\right) + B_D \nabla_H^4 (T)$$

$$\frac{\partial S}{\partial t} + L(S) = \frac{\partial}{\partial z}\left(K_D \frac{\partial S}{\partial z} \right) + B_D \nabla_H^4 (S)$$

- density (ρ) in the equation of state $\rho = \rho(S, T, p)$

In order to maintain both computational efficiency and accuracy, a modified version of the Bryan and Cox (1972) equation of state was used to compute density in the Arctic Ocean. It was modified to best fit the full UNESCO equation of state (Bryan and Cox use a polynomial fit to the Knudsen equation (Foffonof, 1962)). Details of that approach can be found in Parsons (1995).

The following variables contained in the above equations are defined as: model longitude λ, model latitude φ, depth z, time t, Earth's radius a, gravity acceleration g, mean density ρ_o, Coriolis parameter $f = 2\Omega \sin\Phi$ where Ω is the Earth's angular rotation speed and Φ is the true geographical latitude, biharmonic horizontal eddy viscosity $B_M = -2 \times 10^{19} cm^4 s^{-1}$ and diffusivity $B_D = -4 \times 10^{19} cm^4 s^{-1}$ coefficients, and vertical eddy viscosity K_M and diffusivity K_D coefficients. The coefficients for vertical mixing are calculated as a function of Richardson number using a modified Munk and Anderson (1948) approach with guidance adopted from Brooks (1994) and Endoh et al. (1981). The advection operator is defined as

$$L(\sigma) = \frac{1}{a\cos\varphi}\frac{\partial}{\partial\lambda}(u\sigma) + \frac{1}{a\cos\varphi}\frac{\partial}{\partial\varphi}(v\sigma\cos\varphi) + \frac{\partial}{\partial z}(w\sigma)$$

The horizontal Laplacian operator is

$$\nabla_H^2 \sigma = \frac{1}{a^2\cos^2\varphi}\frac{\partial^2\sigma}{\partial\lambda^2} + \frac{1}{a^2\cos\varphi}\frac{\partial}{\partial\varphi}\left(\cos\varphi \frac{\partial\sigma}{\partial\varphi} \right)$$

and the horizontal biharmonic operator is

$$\nabla_H^4 \sigma = \frac{1}{a^2\cos^2\varphi}\frac{\partial^2}{\partial\lambda^2}\nabla_H^2\sigma + \frac{1}{a^2\cos\varphi}\frac{\partial}{\partial\varphi}\left(\cos\varphi \frac{\partial}{\partial\varphi}\nabla_H^2\sigma \right)$$

where σ is a dummy variable and subscripts M and D denote momentum and diffusion respectively.

The model boundary conditions are briefly summarized as follows. At the lateral walls no-

slip boundary conditions are imposed for momentum (u=v=0). For temperature and salinity, no-flux conditions apply ($(\partial\sigma)/(\partial n) = 0$, where σ is either temperature or salinity and n is the direction normal to the boundary). To use the biharmonic horizontal mixing parametrization, additional boundary conditions are required for momentum ($\nabla^2 u = \nabla^2 v = 0$) and for temperature and salinity ($(\partial\nabla^2\sigma)/(\partial n) = 0$). At the surface, wind stress fields are specified from twice-daily analyses of the European Centre for Medium-Range Weather Forecast (ECMWF), averaged over 3-day intervals for the period of 1992. The heat and buoyancy fluxes were parameterized by restoring the surface temperature and salinity toward monthly mean climatologies (Levitus et al., 1994), with a relaxation time scale of one month. Similar restoring is also used along the vertical boundaries in the North Atlantic and Bering Strait where the model domain has been closed.

The vertical velocity at the surface is a function of the sea surface height η: $w = (\partial\eta)/(\partial z)$ at z=0. By allowing a free-surface (η), the model is required to explicitly solve both the baroclinic and barotropic components of motion. The details of this approach are found in Killworth et al. (1991). Implementation of a free surface allows the model to have realistic unsmoothed bathymetry, which together with high resolution (1/6° or ~18 km in rotated coordinates and 30 levels) makes it possible to retain the Canadian Archipelago and other small islands (Figure 1). Small topographic features were omitted or smoothed in previous modeling studies of the Arctic Ocean (i.e. Hibler and Bryan, 1987; Semtner, 1987; Riedlinger and Preller, 1991; Hakkinen, 1993). Keeping in mind that local processes of basin-wide importance are often controlled by small-scale topographic features, the accurate Arctic Ocean bathymetry of this model provides a foundation for more realistic simulations.

At the bottom the flow is required to follow the slope of the bathymetry

$$w = -\frac{u}{a\cos\varphi}\frac{\partial H}{\partial\lambda} - \frac{v}{a}\frac{\partial H}{\partial\varphi} \text{ at z=-H } (\lambda, \varphi)$$

and no heat or salt fluxes are allowed through the bottom. A quadratic approximation of bottom stress is used

$$\vec{\tau}_b = \rho C_D \frac{\vec{U}|\vec{U}|}{d^2}$$

where $\vec{U}$ is the bottom total velocity vector, $C_D = 4 \times 10^{-3}$ is a bottom drag coefficient, and d is the thickness of the bottom layer.

3. Ocean General Circulation

In order to adequately understand the important physical results in an Arctic simulation both circulation and density structure need to be analyzed at spatial scales ranging from local to basin-wide. To have a full picture, temporal variability must be considered as well. Our discussion here is based on a 6-year integration of the stand-alone ocean model initialized from an annual mean climatology (Levitus 1982) and forced with 1992 wind stresses from the European Centre for Medium-Range Weather Forecasts (ECMWF) and with a monthly mean climatology of temperature and salinity (Levitus et al., 1994). No claims are made here to present an equilibrium state of the ocean circulation and especially density structure. The results described in next sections should rather be viewed as an initial contribution toward better understanding of the distribution of currents and water mass exchanges in the Arctic Ocean from an ongoing modeling study.

Traditionally, models of the Arctic Ocean and sea ice have addressed only the large scale circulation as a consequence of having grid spacings of 100 km or more (Semtner, 1976, 1987; Hibler and Bryan, 1987; Riedlinger and Preller, 1991; Holland, 1993; Weatherly and Walsh, 1996). Although such studies are valuable in the context of exploring some physical issues, a few recent efforts depict the arctic sea ice and ocean circulations with more detail to better represent their complex structures (Zhang and Hibler, 1997; Hakkinen, 1993). These new studies recognize that high model resolution provides more realism

to model simulations, allows better model-to-data comparisons, and helps in developing and testing new parameterizations of subgrid processes for use in lower resolution general circulation models. Our approach is similar: to model the Arctic Ocean and sea ice at increasingly high resolution in three dimensions while using accurate forcing data sets and bathymetry.

We start with the basin-wide distribution of sea level height (Figure 2a) and barotropic flow (Figure 3), which are representative of depth integrated dynamical fields. In Figure 2a, negative heights (shown in blue) are usually associated with cyclonic circulation and positive heights (shown in yellow and red) with anticyclonic circulation. Positive heights can also be seen along the shelf and slope regions, representing piling of water against the continental margins to the right of the flow direction. This is especially the case in the northeastern North Atlantic, along the coast of Norway where the northward flow of Atlantic Water enters the Norwegian Sea, and along the coast of Greenland and Labrador where the outflow from the Arctic Ocean into the Greenland, Irminger, and Labrador Seas occurs. Anticyclonic circulation prevails on the Siberian shelves and in most of the Canadian Basin with maximum heights of 40 cm or more simulated in the Beaufort Sea. A border between positive and negative height regions lies somewhere along the Mendeleyev-Alpha Ridge. This border can probably be displaced either toward the Lomonosov Ridge or southward into the Beaufort Sea depending on interannual variability of the atmospheric circulation, which intensifies or weakens the anticyclonic circulation of the Beaufort Gyre. Cyclonic circulation dominates in the Eurasian and Makarov Basins, in the Barents, Nordic (Greenland, Iceland, Norwegian), Irminger, and Labrador Seas, and in the Baffin and Hudson Bays. Maximum mean negative heights of order -30 cm or more exist in the Labrador, Irminger, and Nordic Seas. Height gradients of order 4×10^{-6} (40 cm over 100 km) are common along the continental slope of Greenland. The sea level field also has surface signatures of such topographic features as the Reykjanes Ridge, Voring Plateau, Bear Island Trough, St. Anna Trough, Lomonosov Ridge, and Morris Jesup Pla-

teau.

The surface eddy kinetic energy field (Figure 2b) shows the western Canadian Basin as the only region of high eddy activity in the otherwise generally not eddy-active central Arctic Ocean. This is in agreement with the viewpoint of Aagaard and Carmack (1994; Figure 4) who suggest that eddies observed in the Central Arctic originate mainly from the margins of the Canadian Basin. Those eddies have diameters in the range 10-20 km and speeds up to 30 cm/s or more (Manley and Hunkins, 1985, D'Asaro, 1988). Of course such small features would require grid sizes less than 18 km to be resolved numerically, nevertheless qualitatively the model can represent and depict regional scale circulations. High eddy kinetic energy also exists in the Norwegian, Greenland, and Labrador Seas and the northern North Atlantic and it will be discussed in next sections.

Figures 3a and 3b show annual mean barotropic speed and mass transport per unit width, respectively. In Figure 3a, details of the barotropic speed field are shown over shelf and slope regions, where depth averaged velocities are relatively high. In Figure 3b, details of barotropic circulation in deep basins are better represented using a variable called 'mass transport per unit width', defined as a product of barotropic speed and local depth. One of the most noticeable features of these two figures is the width of the major currents throughout the Arctic Ocean. These currents are narrow, typically less than 100 km (3-5 grid points). To resolve such flows accurately (with 7-10 grid points), model resolution of ~10 km is needed, a similar scale to the local radius of deformation. It means that not only eddies but also the major currents distributing heat, salt, and water masses in the Arctic Ocean require high resolution to be adequately represented in the model.

In Figure 3a barotropic currents with speeds of several cm/s are most typical, although stronger flows up to ~10 cm/s occur along the continental slopes and on the shelves of Greenland, Labrador, and Norway with maximum of 40 cm/s or more along southern Greenland. Elevated speeds exist along the northern slope of Alaska extending over the

Northwind Ridge and Chukchi Cap, over the Iceland-Scotland Ridge, in the St. Anna Trough, along the continental slope north of Severnaya Zemlya, and at various straits of marginal seas (i.e. Kara Gate, Vilkitsky, Laptev, Donga, Nares, and Hudson Straits).

Barotropic flow is an important component of most major currents throughout the Arctic Ocean. This has already been documented in the Greenland Sea both from field observations (e.g. Foldvik et al., 1988) and by modeling studies (Legutke, 1991; Maslowski, 1996). Our simulations indicate that barotropic currents contribute significantly to the large scale circulation throughout the Arctic Ocean. A strong topographic control characteristic of barotropic flow is evident in the Eurasian and Canadian Basins and in the Arctic marginal seas, where relatively strong transports are confined mainly to the continental slopes (Figure 3b). In the central Arctic, some recirculation occurs along the Nansen, Lomonosov, and Mendeleyev-Alpha Ridges within each basin. Relatively strong barotropic flow exists also around other topographic features whose signatures are seen in the height field of Figure 2 (Reykjanes Ridge, Voring Plateau, Bear Island and St. Anna Troughs, and Morris Jesup Plateau). At regional scales, the barotropic velocity field (Figures 3a-b) includes such features as the Jan Mayen, Irminger, and North and East Icelandic Currents, branching of the West Spitsbergen and West Greenland Currents, and recirculation within the Baffin Bay and the Beaufort, Greenland, Irminger, and Labrador Seas. These and other aspects of some regional circulations are discussed next.

Section 4. Regional Ocean Circulations

To describe circulations in all marginal seas and deep basins that are included in the model domain is beyond the scope of one paper. The next sections will concentrate on the following three regions: 1) northern North Atlantic and Labrador Sea, 2) Nordic Seas, and 3) Barents Sea. To describe circulations there we will use global foldout maps of velocity vectors fields at three depth ranges: i) surface 0-45 m (Plate 1), ii) Atlantic layer 180-440

m (Plate 2), and intermediate layers 1100-1700 m (Plate 3). Additionally various vertical cross sections are used. Velocity vectors in Plate 1-3 are averaged in depth (over each depth range) and in time (over 366 days of 1992) and are shown at every grid point to adequately depict narrow currents in a complicated geometry. Because of the averaging over a period of only one year, some of the meanders and eddies in the plates are remnants of time-dependent circulations rather than long-term mean features. In each plate strong currents appear at first glance as dark ribbons over background grey weak currents. In Plate 1-3, a unit vector (0.5 cm) represents a flow at 20, 10, and 5 cm/s respectively. The maps have been chosen such as to show maximum information possible within the limitations of journal publication. More quantitative information can be obtained from larger velocity maps which are available on request. Because of the short time integration, deep circulation is not discussed much at this time.

4.1 Northern North Atlantic and Labrador Sea

Starting in the northern North Atlantic, two cyclonic gyres are recognized on each side of the Reykjanes Ridge: one in the Irminger Basin on the western side and another one in the Iceland Basin on the eastern side of the ridge. The Irminger Sea cyclonic gyre is connected to the Labrador Sea circulation in two ways: (i) the East Greenland Current becomes the West Greenland Current after it passes along the southern tip of Greenland; and (ii) some recirculating northeastward flow from the southern Labrador Sea passes south of Greenland and becomes the Irminger Current flowing northward along the western slope of the Reykjanes Ridge. The core of this last current follows approximately the 2000 m isobath. As it recirculates to the south, the Irminger Current stays separated from the East Greenland Current, which flows further up the shelf slope after passing south through Denmark Strait. The two currents converge at about 60° N to become the West Greenland Current passing Cape Farewell. This current recirculates within the northern

Labrador Sea in two main branches south of 65° N, following the continental margins of the Labrador Basin. Some northwestward flow exists further to the north into Davis Strait and it merges with the southward outflow from the Baffin Bay to enter Hudson Strait to the west. The Labrador Current carries the bulk of water to the south along the west side of the Labrador Sea out into the North Atlantic. Somewhere between $54 - 55^o$N, a portion of this current meanders off to the northeast, toward Greenland to enter the Irminger Sea and continue north as the Irminger Current.

On the other side of the Reykjanes Ridge, the cyclonic circulation in the Iceland Basin is the main well-organized feature of the northeastern North Atlantic. After recirculating to the south, a portion of water below the upper layers (Plate 2 and 3) overflows onto the western side of the ridge into the Irminger Basin and turns to the north with the Irminger Current. To the south and east of the Iceland Basin, remnant eddy-like structures exist in the northern North Atlantic (Figure 3). The scales of transient eddies there are probably still not fully represented in the model. From observations (e.g. Krauss et al., 1990) the scale of eddies produced by baroclinic instability in the North Atlantic at $50 - 60^o$N is as small as 10 km.

Three major pathways of Atlantic Water to the north into the Norwegian and Iceland Seas can be distinguished. Two inflows are due to the Irminger Current separating between $61 - 62^o$ N along the Reykjanes Ridge into two branches. One branch enters the Iceland Sea through Denmark Strait west of Iceland, becoming the Irminger-North Icelandic Current; and another branch follows the southeastern coast of Iceland. The latter branch is in part fed by water recirculating below the surface (Plate 2, 3) within the northern Iceland Basin. This distinct branch follows the southeastern coast of Iceland, then continues southeast along the Iceland-Faeroe Ridge, and finally converges with the third main inflow entering the Norwegian Sea through the Faeroe-Shetland Channel to become the Norwegian Atlantic Current (NAC).

The northward flow through Faeroe-Shetland Channel and through Denmark Strait have been recognized since Helland-Hansen and Nansen (1909). The northward transports through Faeroe-Shetland Channel were estimated earlier at 7-8 Sv ($1Sv = 10^6 m^3/s$) and 1-2 Sv through Denmark Strait (Worthington, 1970, 1976; Dietrich et al., 1980). The existence of the third northward inflow, the eastern branch of the Irminger Current, has been recently discussed by Krauss (1995) based on results from a hydrographic section along $62°$ N and movements of about 200 satellite-tracked buoys deployed along this section in the northern North Atlantic during 1981-1989. Many of those buoys followed the eastern branch of the Irminger Current. Some of the buoys deployed to the east of the Reykjanes Ridge first moved as far south as 57 N before turning toward the northeast, suggesting a cyclonic circulation in the Iceland Basin similar to the one described above. Additionally, based on their measurements by Lagrangian drifters at 15 m depth during 1991-1993, Poulain et al. (1996) suggest the presence of a strong and well defined current along the Iceland-Faeroe Frontal zone. Finally, the inflow along the southeastern coast of Iceland is also found in a recent modeling study of Heburn and Johnson (1995), using a two-layer version of the Naval Research Laboratory model (Hurlburt and Thompson, 1980; Wallcraft, 1991) forced with monthly mean wind stress climatology of Hellerman and Rosenstein (1983).

To estimate mass exchanges between the North Atlantic and the Arctic Ocean transport through the three pathways shown in Figure 4a-c are calculated as follows. The southward transport of water colder than $2°$ C at a section to the north of Denmark Strait is about 4.2 Sv decreasing to 3.4 Sv at the sill and down to 2.7 Sv at a section further south near the “Overflow 73” section (Clarke, 1984), where the time-averaged volume flux of water colder than $2°$ C was estimated to be 2.9 Sv. The northward transport of the Irminger Current through Denmark Strait starts from about 1 Sv at the “Overflow 73” section and decreases northward to 0.8 Sv and then to 0.5 Sv. The decrease of transports downstream of each flow can be explained in part by mixing and entrainment of warm northward flow-

ing waters of the Irminger Current into the cold southward flow of Denmark Overflow Water as shown in Figure 4a. Further south of Denmark Strait transport of water colder than 2° C is only 1.7 Sv, but it is about 2.9 Sv for water colder than 4° C. At this temperature regime (T<4° C) dense southward transport at a section about 180 km to the south of the "Overflow 73" section is about 5.7 Sv, increasing to 10.0 Sv at a section 200 km further south, and reaching 13.8 Sv at a section to the south of Cape Farewell. Based on measurements from the available long term current meter arrays between Denmark Strait and Cape Farewell, Dickson and Brown (1994) propose the following transport scheme for waters denser than σ_θ = 27.80: 5.1 Sv at a section 160 km south of Denmark Strait (the 'TTO' Array), 10.7 Sv at a section 160 km further south (the Angmagssalik Array), and 13.3 Sv at Cape Farewell (see Figure 13 of their paper).

The annual mean outflow of dense and cold water (T<3° C) from the Nordic Seas through the Faeroe-Shetland Channel is about 1.0 Sv plus an additional 0.3 Sv between Iceland and Faeroe Island (Figure 4b, c). The inflow of warm Atlantic Water through these two pathways is about 3.9 Sv and 3.1 Sv, respectively. There is no clear indication of seasonal signals in those transports. Simulated variability occurs in each section at timescales of days to weeks, suggesting the presence of eddies as shown in Figure 2b. Earlier estimates of total transports through the Faeroe-Shetland Channel by Tait (1957) based on hydrographic sections from 1927 to 1952 showed 2-3 Sv (ranging from 0.4 to 6.5 Sv). Van Aken (1988) calculated Atlantic Water transport of 1.7 Sv through the Faeroe-Shetland Channel and 6 Sv over the Iceland-Faeroe Ridge. The net transport of the flow continuing in the Norwegian Sea, the NAC, is 7-8 Sv (Worthington, 1970, McCartney and Talley, 1984, Dietrich et al., 1980). This total compares well with the total NAC transport of 7 Sv from the model. The main finding from the above transport calculations though is that only about half of the northward transport occurs through the Faeroe-Shetland Channel; the other half is due to the eastern branch of the Irminger Current.

It is quite possible that some differences in transports through separate sections might be related to model bathymetry, atmospheric forcing of 1992, and a short integration. Additionally, model and real sections are not at exactly the same locations, results are averaged over different time periods, and are not in terms of a specified density range. Despite these differences, it is clear that simulated transports are rather realistic, thus demonstrating the potential for adequate modeling and understanding of water mass exchanges between the Arctic Ocean and the North Atlantic.

4.2 Nordic Seas

As discussed above, Atlantic Water enters the Norwegian Sea via two pathways: i) along the southeastern coast of Iceland then following the Iceland-Faeroe Ridge and ii) through the Faeroe-Shetland Channel (Plates 1 and 2). The two branches converge at the northern end of the Faeroe-Shetland Channel in the southern Norwegian Basin and continue flowing northward as the Norwegian Atlantic Current. Some of the flow through the Faeroe-Shetland Channel turns to the east and then to the northeast as it joins the Norwegian Coastal Current, which is confined to the coast and shelf of Norway (Saetre and Mork, 1981). The NAC in the deep Norwegian Basin parallels the Norwegian Coastal Current up to about 65°N and then turns to the north following the southern slope of Voring Plateau and the Jan Mayen Fracture Zone. The bulk of this current overflows the fracture zone at about 70°N then turns to the southeast along the northern side of the fracture zone and the northern slope of Voring Plateau in the Lofoten Basin. A small part of the overflow through the Jan Mayen Fracture Zone (Plates 1,2) goes to the northeast along the Mohns Ridge in the western Lofoten Basin and joins the West Spitsbergen Current at around 73°N. The total transport of warm water ($T \geq 0°C$) by the NAC including this western branch is 10 Sv, of which the main eastern branch of the current accounts for about 8 Sv. Increased eddy activity exists along the NAC and Norwegian Coastal Current (Figure 2b). The velocity fields in the Lofoten Basin (Plates 1 and 2) have captured a slow-moving ring

of diameter 200 km to the north of Voring Plateau. Its structure and dynamics resembles a warm core ring generated by instability in the Gulf Stream. Further downstream, a well-known narrowing and intensification of the NAC occurs just before the splitting of the NAC near the Lofoten and Vesteraalen Islands.

A similar schematic surface circulation is derived by Poulain et al. (1996) from Lagrangian drifters released in the Nordic Seas between the summer of 1991 and 1993. Following their scheme from the Iceland-Faeroe Frontal Zone through the Norwegian and Lofoten Basins, the flow of NAC and Norwegian Coastal Current and their merging and intensification west of Lofoten and Vesteraalen Islands are adequately represented in the model. The dominant velocities measured in the NAC are between 10 and 40 cm; correspondingly, the simulated annual mean velocities are between 20 and 30 cm/s, increasing to above 30 cm/s near the Lofoten and Vesteraalen Islands. The flow across the Voring Plateau following the shelf slope between the 500 and 1000 m isobaths is weaker and more meandering in the model mean fields than as derived from drifters. Also no organized cyclonic gyre exists in the circulation of the upper Norwegian and Lofoten Basins (Plate 1,2). With 1992 wind forcing, the ocean model does not reproduce a south-eastward flow along the Mohns Ridge in the western Lofoten Basin and a southward flow along the Jan Mayen Ridge in the western Norwegian Basin. The latter flow exists only in the deep Norwegian Basin (Plate 3) as part of a gyre-like cyclonic circulation. This reduced amount of circulation is supported by Johannessen (1986) who argues on the basis of satellite measurements and earlier results against the existence of a large cyclonic gyre in the Norwegian Sea as proposed by Helland-Hansen and Nansen (1909). Instead he suggests a splitting of the NAC into two branches separated by regions where increased eddy activity exists, as is similarly described here. Some of these current patterns need to be revisited in the future using results obtained from a coupled ice-ocean model forced with interannual atmospheric forcing and making comparisons with expanded observations.

The NAC continues northeast along the shelf and slope of Norway until it splits into the North Cape Current entering the Barents Sea and the West Spitsbergen Current continuing north toward Fram Strait. More discussion on the circulation in the Barents Sea follows in the next section. The West Spitsbergen Current (WSC) continues meandering to the north with some branches occasionally overflowing the Knipovich Ridge into the central Greenland Sea (Plates 1,2). Two regions where the overflows occur are between $73 - 74°$, along the northern slopes of the Lofoten Basin, and between $78 - 79°$ N where the Knipovich Ridge joins the shelf slope of western Spitsbergen. Additional recirculation occurs also around $81°$ N and between $82 - 83°$ N. This filamented structure of the northern WSC closely resembles that described by Gascard et al. (1995; see their figure 1, p.132) with the exception of the northernmost branch. In the model the branch forms a closed cyclonic cell centered over the northwestern flank of Yermak Plateau. The bulk of the upper flow of the WSC from Fram Strait (Plates 1,2) follows the path across the Yermak Plateau (branch D in Gascard et al. (1995)) into the Litke Trough and recirculates to the west around the northern Yermak Plateau at about $82°$ N. Calculated annual mean transport of water warmer than $0°$ C in the flow across the Yermak Plateau into the Litke Trough is 4.65 Sv. Part of that flow, about 1.5 Sv continues to the east following the continental slope. Additionally, about 2 Sv of the recirculation around the northern Yermak Plateau separates at ~$83°$ N, and meanders northward into the deep Nansen Basin. Thus the two northward inflows through Fram Strait amount to roughly 3.5 Sv, of which only 1.5 Sv supplies the boundary current along the continental margins carrying Atlantic Water around the Arctic Ocean. The presence of sea ice and interannual forcing in the model could modify this circulation pattern in Fram Strait, but hydrographic and current meter data collected in that region by Muench et al. (1992) during March-April 1989 and by Manley et al. (1992) over an 11-year period, describe a very similar recirculation regime around the northern Yermak Plateau.

Figures 5a-b show annual mean temperature and salinity sections through Fram Strait (along the model coordinate x=156, so the western part starts at ~82° N, the eastern part ends at ~78° N, and it passes through 80° N in the middle). Northward flow of Atlantic Water consists of two cores: a warm ($T_{max} > 6°$ C) and saline ($S_{max} > 35.1$) branch following the continental slope and a cooler ($T_{max} \sim 5°$ C) and less saline ($S_{max} \approx 35.05$) offshore branch. Along the eastern side of the strait, waters with temperature well above 0° C extend from the surface down to 800-900 m. On the western side, waters leaving the Arctic Ocean at that depth range (except for the upper 200 m where Polar Water ($T < 0°$ C, $S < 34.5$) resides) are still relatively warm with T=0 – 0.5° C and S=34.5 – 34.9. A deep saline maximum exists along the western side (Figure 5b) with the core between 1500-2500 m, salinity $S > 34.94$, and temperature $T \sim -0.5°$ C which is typical for Arctic Ocean Deep Water (Aagaard et al., 1985, Smethie et al., 1988, Swift and Koltermann, 1988). Examination of the simulated flow at this depth (not shown) indicates continuing outflow of high salinity water from the central Arctic.

Transport of the EGC before entering Fram Strait and before receiving any recirculation from the WSC is about 6 Sv. This transport remains about the same until 79° N, where the main recirculation branch of the WSC is known to join the EGC (Bourke et al., 1988). Annual mean velocities up to 20 cm/s or more exist there and about 4.5 Sv of the flow is contained in the upper 700 m. This is higher than a transport of 3 Sv calculated by Foldvik et al. (1988) based on a year-long current measurements but it is less than an estimate by Aagaard and Greisman (1975) of 5.3 Sv of recirculating Atlantic Water. It is interesting to note that the total transport of 7.1 Sv calculated by Aagaard and Greisman (1975) contains the same amount of Atlantic Water (i.e. 75%) as the total transport in the model does. Again, it could be argued that our transports may change in a coupled ice-ocean model, but it is also possible that the transport calculated by Foldvik et al. (1988) (using extrapolated upward velocities in the upper 100 m) is an underestimate. Their velocity section shows the maximum southward flow of only ~14 cm/s in the upper layer which is less than

the maximum annual mean speeds of 20 cm/s in the model and it is less than the speeds of 20-40 cm/s in the upper 100 m as measured by a drifting buoy in summer (see Figure 5 in Foldvik et al., 1988).

Further to the south, after being joined by the two already described recirculation branches from the WSC, the transport of the EGC increases to ~10 Sv (section along x=190). Out of this total about 8 Sv flows above the 700 m depth, 1.5 Sv of which is confined over the shelf, and the maximum velocity in the upper layer is still above 20 cm/s. The mean June 1992 salinity section there shows Atlantic Water recirculating within the EGC at depth range roughly 200-700 m along the continental slope (Figure 6a). The second salinity maximum, representing the deep Arctic Ocean outflow already seen in Fram Strait (Figure 5b), occupies depths between 800-2200 m. Its center with maximum of ~34.925 is located at about 1200 m. To show model skill, we compare this figure to roughly the same section obtained from the annual mean Levitus data, which was used to initialize the model. Those two figures in turn can be compared against the hydrographic sections at similar locations obtained from the R/V Polarstern in June 1987 (Aagaard et al., 1991, Strass et al., 1993). The model section compares quite favorably with the one from observations (see Figure 2 in Strass et al., 1993) with two salinity maxima, one at depths of about 100 to 800 m and the maximum above 34.95 and second between about 1000 and 2500 m. The latter salinity maximum is discussed by Aagaard et al. (1991) and for the best comparison our model section (Figure 6a) is chosen close to their section across the Greenland slope between 74 and 76° N (see their Figures 1 and 2). Aagaard et al. (1991) find the deep outflow from the Arctic Ocean at depths 800-2400 m and its core with salinities up to 34.919 is centered near 1200 m. Our section (Figure 6a) does not show the details of the vertical structure, but it quite realistically represents this deep water outflow from the Arctic Ocean. Compared with the section from the annual mean Levitus data (Figure 6b) the model is much different from the initial data and within the limitation of resolution and forcing fields it is close to real conditions there.

Between 73 and 72° N the Jan Mayen Current (JMC) separates off the EGC and closes the cyclonic gyre of the Greenland Basin from the south (Plates 1 and 2). The surface signature of the JMC (Plate 1) clearly shows that it originates from a large meander in the EGC, the bulk of which turns south before Jan Mayen Island and joins the main branch of EGC further to the south in the Iceland Sea. This situation changes with depth (Plate 2 and 3) where, due to increased topographic steering, more water continues eastward along the Jan Mayen Fracture Zone and less turns south onto Iceland Plateau. Both an earlier measurement in that area (Bourke et al., 1992) and a modeling study (Legutke, 1991) describe a similar wide meander in the EGC and similar behavior with depth.

4.3 Barents Sea

The North Cape Current separating off the NAC enters the Barents Sea as a relatively wide flow contained between the southern part of Bear Island Trough and the coast of Norway (Plates 1 and 2). Looking at the section between Norway and Spitsbergen (Figure 7) and at Plate 1, two branches are distinguished within the North Cape Current: one closer to the coast of Norway and second along the southern Bear Island Trough. Both plane view (Plates 1 and 2) and the section (Figure 7) clearly show a recirculation of warm Norwegian Atlantic Water (T=2 – 8° C; S>35.0) within the trough. Additionally, recirculation also occurs between Bear Island and Svalbard. Annual mean velocities across the trough are above 17 cm/s into and 4 cm/s out of the through. The total transport in through the section of Figure 7 is about 3.1 Sv into and 0.9 Sv out of the Barents Sea, resulting in the net NAC inflow of 2.2 Sv. This compares well with earlier estimates of 2 Sv by Rudels (1987) and with 3 Sv inflow with about 1 Sv outflow by Blindheim (1989).

The Barents Sea circulation and in particular the recirculation of Norwegian Atlantic Water inside the Bear Island Trough was of primary interest in our early modeling efforts, since the data collected in summer of 1992 in that region (Parsons et al., 1996) provided a direct opportunity for comparison with the model results at smaller scales. Three model-

ing experiments, including i) annual mean forcing, ii) annual mean forcing coupled with semidiurnal tidal forcing, and iii) and seasonal forcing, were conducted to simulate conditions observed in 1992. Details of that comparison are discussed by Parsons (1995) and they are only summarized here. All three experiments predicted the recirculation of Norwegian Atlantic Water within Bear Island Trough, consistent with the observed circulation pattern. The unique 3-dimensional tidal forcing experiment highlighted the significance of including tides in shallow seas simulations. Significant changes in the temperature and salinity structure due to tidal mixing were seen throughout the Barents Sea when compared to simulations without tides. Overall, the resultant T-S structure more closely resembled the available observations. This was attributed to the effect of tidally induced residual flow. Tidally induced residual flows also had the effect of reducing the simulated net volume transport of the NAC into the Barents Sea by 0.4 Sv, bringing it closer to observed estimates. Finally, ocean model results indicated that at smaller scales sea ice and more realistic buoyancy fluxes are needed in order to more adequately represent conditions there. For example, the coherent advection of Barents Polar Water (-1° to 6°C and S<34.4) to the known frontal summertime position is contingent upon strong surface stratification of the upper layers from the summer ice melt. Thus the presence of sea ice over the Barents Sea in the preceding winter is a necessary condition even for a summertime simulation.

Here we concentrate on the larger scale Barents Sea circulation and transport estimates in and out of this region. The coastal branch of the North Cape Current continues eastward somewhere along the 200 m isobath and reaches the longitude of Murmansk before it separates off the coast toward Novaya Zemlya and then follows the northwestern side of this island. Pfirman et al. (1994) describe a similar observed circulation and define the Norwegian part of this current as the Norwegian/Murmansk Coastal Current and the part along Novaya Zemlya as the Novaya Zemlya Current. Between the coast of Norway and Novaya Zemlya, part of this flow turns onto the shallow (< 100 m) shelf to the southeast to over-

flow into the Kara Sea through Kara Gate. The eastward transport calculated there is 0.2 Sv; and it is within the range of 0.04-0.6 Sv as estimated from earlier Russian observations and modeling (Pavlov et al., 1996).

The other branch of the North Cape Current, entering along the southern bank of Bear Island Trough, continues in the deeper Barents Sea meandering eastward toward Novaya Zemlya and then northward. Most of this flow leaves the shelf via St. Anna Trough. The flow taking this particular route merges with water carried by the Novaya Zemlya Current, and its transport before entering the trough is about 1 Sv. Some flow turns to the north earlier before reaching Novaya Zemlya and leaves the shelf between Spitsbergen and Franz Josef Land.

Within St. Anna Trough a major recirculation occurs. The bulk of warm Atlantic Water carried along the continental margin from Fram Strait enters the trough to the south, merges with the cooler and more saline outflow from the Barents Sea, and recirculates back as shown in the sections of Figure 8. Relatively strong opposite currents exist within the trough which in its narrowest parts is only about 150 km wide. Annual mean velocities there (Figure 8) are above 10 cm/s both in and out of the trough. The respective transports calculated there are 1.5 Sv in and 2.5 Sv out, which amounts to a net outflow of 1 Sv from the Barents Sea and accounts for the transport calculated in the section west of Novaya Zemlya before St. Anna Trough.

Before reaching St. Anna Trough, the flow originating from Fram Strait recirculates in a few smaller troughs along the shelf break between Spitsbergen and Franz Josef Land. Recirculation is weaker there than in St. Anna Trough, but it is still quite significant in the overall exchange of waters between the Barents Sea and the Arctic Ocean. The total there is about 0.3 Sv in and 1 Sv out, adding a significant 0.7 Sv of net outflow into the boundary current continuing along the shelf slope. Finally, closing the mass transport budget within the Barents Sea, there is a net outflow of about 0.4 Sv to the east of St. Anna

Trough and less than 0.1 Sv through Vilkitsky Strait into the Laptev Sea. Based on regional model results and earlier measurements, Pavlov et al. (1996) estimate that between 0.16 and 0.3 Sv exits the Kara Sea through Vilkitsky Strait.

Summarizing the model results, about 1.5 Sv inflow through Fram Strait and more than 2 Sv of water out from the Barents Sea supplies the narrow boundary current following the continental margins in the Arctic Ocean. Additionally 2 Sv of water enters through Fram Strait into the deep Nansen Basin and it does not feed the flow along the slope. Hence, when comparing the sources of the boundary flow, these results confirm indications from recent observations (Rudels 1994) that the Barents Sea contribution may be as great as, or perhaps greater than, the contribution by the West Spitsbergen Current.

5. Summary and Conclusions

The previous sections have described the development and early use of a high-resolution model of the Arctic Ocean and subpolar North Atlantic. Not only does the free-surface model have high resolution in three space dimensions, but it also has more accurate coastlines and bathymetry than was previously permissible in rigid-lid models. This has allowed narrow straits, sills, canyons, and even the Canadian Archipelago to be accurately depicted. Using observed 1992 atmospheric forcing, prescribed temperature and salinity in a mid-latitude boundary zone, and grossly defined initial Levitus conditions, we conducted a 6-year simulation of ocean circulation in the Arctic Ocean, its marginal seas, and the northern North Atlantic.

The simulated ocean circulation is dominated by narrow currents typically less than 100 km in width, which are steered by bottom topography and become hydrodynamically unstable in certain areas. Although the 18-km grid spacing is somewhat marginal for treating the eddies, it nevertheless is useful for providing a first-ever estimate of eddy activity

throughout the Arctic, in the absence of a corresponding observational product. The representation of the mean currents is more adequately handled by the present grid spacing; and many specifics of complex interconnected flows around basins and within marginal seas have been successfully validated by observations. This provides a new basis for understanding the overall connectivity of Arctic circulation beyond what is possible from observations alone. In particular, the present simulation has reproduced the overflow characteristics exiting the Nordic Seas, the detailed characteristics of the Norwegian Atlantic Current along most of its path, and the complex interactions of the opposing currents in and around Fram Strait. Based on those successes, greater confidence can be placed in other aspects of the simulations regarding net transports by the various currents and the circulations in less densely observed regions such as north of Spitsbergen, in the Barents and Kara Seas, and in the St. Anna Trough.

The present paper covers the development of only the ocean model, part II (Zhang et al., 1997) treats the ice-model development and results with ocean model forcing, and part III will discuss coupling to the ocean and simulations with 1990-94 atmospheric forcing. These studies are intended to set the stage for further research involving better forcing fields and better connectivity to the rest of the global ocean. In particular, we have access to the reanalyzed ECMWF products of 1979-93 which, together with the operational products beyond 1993, provide nearly two decades of atmospheric forcing to simulate the overall circulation of water and sea ice in the Arctic, as well as their natural variabilities in climatic terms. Furthermore, another model for the remainder of the global ocean, which has a grid size of about 18 km in a region overlapping the boundaries of the Arctic / subpolar North Atlantic model, is now coupled to the present model for truly global ocean and ice studies. In fact, the anticipated computational upgrades of the next few years will allow century scale integrations of the global and Arctic models, which will then permit the entire thermohaline structure of the Arctic Ocean to be established from idealized initial states and evaluated against a growing observational base. Thereupon, further

improvements in model resolution and in the representation of physical processes will lead to new quantitative understanding of the Arctic Ocean and of its influence on global circulation and variability.

Acknowledgments

This research was supported in part by the DOE CHAMMP Program for ocean and climate modeling, by the NOAA Postdoctoral Program in Climate and Global Change (W.M. and Y.Z.), by the Cray Research and University of Alaska Research and Development Grant Program (W.M.), by the NSF ARCSS Program for the Arctic System study, and by the ONR Fellowship Grant N0001492AF00002 (A.R.P.). Computer resources were provided by the Arctic Region Supercomputing Center at the University of Alaska Fairbanks and by Climate Simulation Laboratory of the National Center for Atmospheric Research.

REFERENCES

Aagaard, K. and P. Greisman, Toward new mass and heat budgets for the Arctic Ocean, J. Geophys. Res., 80, 3821-3827, 1975.

Aagaard, K., J. H. Swift, E. C. Carmack, Thermohaline circulation in the Arctic mediterranean seas, J. Geophys. Res., 90, 4833-4846, 1985.

Aagaard, K., and E. C. Carmack, The role of sea ice and other fresh water in the Arctic circulation, J. Geophys. Res., 94, 14,485-14,498, 1989.

Aagaard, K., E. Fahrbach, J. Meincke, and J. H. Swift, Saline outflow from the Arctic Ocean: Its contribution to the deep waters of the Greenland, Norwegian, and Iceland Seas, J. Geophys. Res., 96, 20,433-20,441, 1991.

Aagaard, K., and E. C. Carmack, The Arctic Ocean and climate: A perspective, In: The Polar Oceans and Their Role in Shaping the Global Environment: The Nansen Centennial Volume, Geophys. Monogr. Ser., Vol. 85, edited by O.M. Johannessen, R. D. Muench, and J. E. Overland, pp. 5-20. AGU, Washington, D.C, 1994.

Blindheim, J., Cascading of Barents Sea bottom water into the Norwegian Sea, Rapp. P.-V. Reun. Cons. Int. Explor. Mer., 188, 49-58, 1989.

Bourke, R. H., A. M. Weigel, and R. G. Paquette, The westward turning branch of the West Spitsbergen Current, J. Geophys. Res., 93, 14,065-14,077, 1988.

Bourke, R. H., R. G. Paquette, and R. F. Blythe, The Jan Mayen Current of the Greenland Sea, J. Geophys. Res., 97, 7241-7250, 1992.

Broecker, W. S., The Great Ocean Conveyor. Oceanography, Vol. 4, No. 2, 79-89, 1991.

Brooks, D. A., A model study of the buoyancy-driven circulation in the Gulf of Maine, J. Phys. Oceangr., 24, 2387-2412, 1994.

Bryan, F., High-latitude salinity effects and interhemispheric thermohaline circulations, Nature, 323, 301-304, 1986.

Bryan, K. and M. Cox, An approximate equation of state for numerical models of ocean circulation, J. Phys. Oceangr., 2, 510-514, 1972.

Clarke, R. A., Transport through the Cape Farewell-Flemish Cap section, Rapp. P-V. Reun. Cons. Int. Explor. Mer., 185, 120-130, 1984.

D'Asaro, E. A., Observations of small eddies in the Beaufort Sea, J. Geophys. Res., 93, 6669-6684, 1988.

Dickson, R. R., J. Meincke, S-A. Malmberg, and A. J. Lee, The "Great Salinity Anomaly" in the Northern North Atlantic 1968-1982, Prog. Oceanog., 20, 103-151, 1988.

Dickson, R. R., and J. Brown, The production of North Atlantic Deep Water: Sources, rates, and pathways, J. Geophys. Res., 99, 12,319-12,341, 1984.

Dietrich, G., K. Kalle, W. Krauss, and G. Siedler, General Oceanography, An Introduction, 2nd ed., 626 pp, edited by John Wiley, New York, 1980.

Endoh, M. C., C. N. K. Mooers, and W. R. Johnson, A coastal upwelling circulation model with eddy viscosity depending upon Richardson Number, In: Coastal Upwelling, Coastal and Estuarine Sciences, No. 1, edited by F. A. Richards, pp. 203-208, AGU, Washington, D.C., 1981.

Fofonoff, N. P., Physical properties of sea water, In: The Sea, Vol 1, 864 pp., Interscience, New York, 1962.

Foldvik, A., K. Aagaard, and T. Torresen, On the velocity field of the East Greenland Current, Deep-Sea Res., 35, 1335-1354, 1988.

Gascard, J.-C., C. Richez, and C. Rouault, New insights on large-scale oceanography in Fram Strait: The West Spitsbergen Current, In: Arctic Oceanography: Marginal Ice Zones and Continental Shelves, Coastal and Estuarine Studies, edited by W. O. Smith, Jr. and J. M. Grebmeier, 131-182 pp., 1995.

Hakkinen, S., An Arctic source for the Great Salinity Anomaly: A simulation of the Arctic ice-ocean system for 1955-1975, J. Geophys. Res., 98, 16,397-16410, 1993.

Heburn, G. W., C. D. Johnson, Simulations of the mesoscale circulation of the Greenland-Iceland-Norwegian Seas, J. Geophys. Res., 100, 4921-4941, 1995.

Helland-Hansen, B., and F. Nansen, The Norwegian Sea, Rep. Norw. Fish. Mar. Inves., II(2), 390 pp., and suppl., 1909.

Hellerman, S., and M. Rosenstein, Normal monthly wind stress over world ocean with error estimates, J. Phys. Oceanogr., 13, 1093-1104, 1983.

Hibler, W. D., III, and K. Bryan, A diagnostic ice-ocean model, J. Phys. Oceanogr., 17, 987-1015, 1987.

Holland, D. M., Numerical Simulation of the Arctic Sea ice and ocean circulation, Rep. 93-4, Ph.D. thesis, 400 pp., Cent. for Clim. and Global Change Res., McGill Univ., Montreal, 1993.

Hurlburt, H. E., and J. D. Thompson, A numerical study of Loop Current intrusions and eddy shedding, J. Phys. Oceanogr., 17, 1909-1924, 1987.

Johannessen, O. M., Brief overview of the physical oceanography, In: The Nordic Seas, edited by B. G. Hurdle, Springer-Verlag, pp. 103-127, 1986.

Killworth, P. D., D. Stainforth, D. J. Webb, and S. M. Paterson, The development of a free-surface Bryan-Cox-Semtner ocean model, J. Phys. Oceanogr., 21, 1333-1348, 1991.

Krauss, W., R. Doscher, A. Lehmann, and T. Viehoff, On eddy scales in the eastern and norther North Atlantic Ocean as a function of latitude, J. Geophys. Res., 95, 18,049-18,056, 1990.

Krauss, W., Currents and mixing in the Irminger Sea and in the Iceland Basin, J. Geophys. Res., 100, 10,851-10,871, 1995.

Legutke, S., A numerical investigation of the circulation in the Greenland and Norwegian Sea, J. Phys. Oceanogr., 21, 118-148, 1991.

Levitus, S., Climatological Atlas of the World Ocean, NOAA Prof. Paper No. 13, U. S. Govt. Print.

Office, 173 pp., 1982.

Levitus, S., R. Burgett, and T. P. Boyer, World Ocean Atlas 1994, Volume 3: Salinity and Volume 4: Temperature, NOAA Atlas NESDIS 3 and 4, U. S. Dept. of Commerce, Washington, 99 and 117 pp., 1994.

Manley, T. O., and K. Hunkins, Mesoscale eddies of the Arctic Ocean, J. Geophys. Res., 90, 4911-4930, 1985.

Manley, T. O., R. H. Bourke, and K. L. Hunkins, Near-surface circulation over the Yermak Plateau in the northern Fram Strait, J. Mar. Syst., 3, 107-125, 1992.

Maslowski, W., and A. J. Semtner, The Great Salinity Anomaly Propagation in the Greenland Sea - Model results, Nordic Seas Symposium, Extended Abstr. Vol., pp. 139-142, Univ. Hamburg, Hamburg, 1995.

Maslowski, W., Numerical simulations of topographic Rossby waves along the East Greenland Front, J. Geophys. Res., 101, 8775-8787, 1996.

McCartney, M. S., and L. D. Talley, Warm-to-cold water conversion in the northern North Atlantic Ocean, J. Phys. Oceanogr., 14, 922-935, 1984.

Meincke, J., et al., Greenland Sea Project, 1990: A venture toward improved understanding of oceans' role in climate, EOS Transactions, 71, No. 24, 750-751.

Mesinger, F., and A. Arakawa, Numerical methods used in atmospheric models, Volume 1, pp. 64, GARP Publication Series 17, WMO-ICSU Joint Organizing Committee, 1976.

Muench, R. D., M. G. McPhee, C. A. Paulson, and J. H. Morison, Winter oceanographic conditions in the Fram Strait-Yermak Plateau region, J. Geophys. Res., 97, 3469-3484, 1992.

Munk, W. H., and E. R. Anderson, Notes on a theory of the thermocline, J. Mar. Res., 7, 276-295, 1948.

Parsons, A. R., On the Barents Sea polar front in summer and interpretations of the associated regional oceanography using an Arctic Ocean general circulation model, Ph.D. thesis, Naval Postgraduate School, Monterey, 185 pp., 1995.

Parsons, A. R., R. H. Bourke, R. D. Muench, C-S Chiu, J. F. Lynch, J. H. Miller, A. J. Plueddemann, and R. Pawlowicz, The Barents Sea Polar Front in summer, J. Geophys. Res., 101, 14,201-14,221, 1996.

Pavlov, V. K., L. A. Timokhov, G. A. Baskakov, M. Yu. Kulakov, V. K. Kurazhov, P. V. Pavlov, S. V. Pivovarov, and V. V. Stanovoy, Hydrometeorological regime of the Kara, Laptev, and East-Siberian Seas, Tech. Mem. APL-UW TM1-96, Univ. of Washington, Seattle, 179 pp., 1996.

Pfirman, S. L., D. Bauch, and T. Gammelsrod, The norther Barents Sea: Water mass distribution and modification, In: The Polar Oceans and Their Role in Shaping the Global Environment: The Nansen Centennial Volume, Geophys. Monogr. Ser., Vol. 85, edited by O.M. Johannessen, R. D. Muench, and J. E. Overland, pp. 77-94. AGU, Washington, D.C, 1994

Poulain, P. M., A. Warn-Varnas, and P. P. Niiler, Near-surface circulation of the Nordic seas as measured by Lagrangian drifters, J. Geophys. Res., 101, 18,237-18,258, 1996.

Riedlinger, S. H., and R. H. Preller, The development of a coupled ice-ocean model for forecasting ice conditions in the Arctic, J. Geophys. Res., 96, 16,955-16,977, 1991.

Rudels, B., On the mass balance of the Polar Ocean, with special emphasis on the Fram Strait, Norsk Polarinstitutt Skrifter, 188, 1-53, 1987.

Saetre, R., and M. Mork, The Norwegian Coastal Current, Proceedings of the Norwegian Coastal Current Symposium, GEILO, 9-12 September 1980, University of Bergen, 1981.

Semtner, A. J., An oceanic general circulation model with bottom topography, Tech. Rep. 9, University of California, Los Angeles, 99 pp., 1974.

Semtner, A. J., Numerical simulation of the Arctic Ocean circulation, J. Phys. Oceanogr., 6, 409-425, 1976.

Semtner, A. J., A numerical study of sea ice and ocean circulation in the Arctic, J. Phys. Oceanogr., 17, 1077-1099, 1987.

Semtner, A. J., and R. M. Chervin, A simulation of the global ocean circulation with resolved eddies, J. Geophys. Res., 93, 15502-15522, 1988.

Semtner, A. J., Modeling ocean circulation. Science, 269, 1379-1385, 1995.

Smethie, W. M., Jr., D. W. Chipman, J. H. Swift, and K. P. Koltermann, Chlorofluoromethanes in the arctic mediterranean seas: Evidence for formation of bottom water in the Eurasian Basin and deep-water exchange through Fram Strait, Deep Sea Res., 35, 347-369, 1988.

Strass, V. H., E. Fahrbach, U. Schauer, and L. Sellmann, Formation of Denmark Strait overflow water by mixing in the East Greenland Current, J. Geophys. Res., 98, 6907-6919, 1993.

Swift, J. H., and K. P. Koltermann, The origin of Norwegian Sea deep water, J. Geophys. Res., 93, 3563-3569, 1988.

Tait, J. B., Hydrography of the Faroe-Shetland Channel 1927-1952, Mar. Res., no. 2, 1-309, 1957.

van Aken, H. M., Transports of water masses through the Faroese Channels determined by an inverse method, Deep Sea Res., 35, 595-617, 1988.

Wallcraft, A. J., The Navy layered ocean model users' guide, NOARL Rep. 35, 21 pp., Nav. Oceanogr. and Atmos. Res. Lab., Stennis Space Center, Miss., 1991.

Weatherly, J., and J. E. Walsh, The effects of precipitation and river runoff in a coupled ice-ocean model of the Arctic, Climate Dynamics, submitted 1996.

Worthington, L. V., The Norwegian Sea as a mediterranean basin, Deep Sea Res., 17, 77-84, 1970.

Worthington, L. V., On the North Atlantic circulation, Johns Hopkins Oceanogr. Stud., 6, 110 pp., 1976.

Zhang, J., and W. D. Hibler, III, On an efficient numerical method for modeling sea ice dynamics, J. Geophys. Res. in print 1997.

Zhang, Y., W. Maslowski, and A. J. Semtner, High resolution Arctic Ocean and sea ice simulations. Part II: Ice model design and early results, J. Geophys. Res., submitted 1997.

Figure Captions

Figure 1. Arctic model domain. Contour lines show isobaths of 300 and 2000 m.

Figure 2. Annual mean (a) sea level height (cm) and (b) surface (0-20 m) eddy kinetic energy (cm^2/s^2).

Figure 3. Annual mean (a) barotropic velocity in cm/s. Contour line shows velocity of 3 cm/s and (b) mass transport per unit width (cm^2/s).

Figure 4. Annual mean temperature in $°C$ (color background) and velocity in cm/s (positive southward) sections along the Greenland-Iceland-Scotland Ridge: (a) Denmark Strait (x=252), (b) Iceland-Faeroe (x=253), and (c) Faeroe-Shetland (x=245).

Figure 5. Annual mean section across Fram Strait (x=156): (a) salinity (ppt) and (b) temperature ($°C$).

Figure 6. Mean June salinity section from (a) the model along x=187 and (b) the World Ocean Atlas (Levitus et al., 1994) along $74.5°$ N - annual mean climatology.

Figure 7. Annual mean temperature in $°C$ and velocity in cm/s (negative eastward) section between Norway, Bear Island, and Spitsbergen (x=154).

Figure 8. Annual mean temperature in $°C$ and velocity in cm/s (positive southward) sections at y=201 (top), 193 (second from the top), 188 (third from the top), and 183 (bottom). Contour intervals for velocity are 2 cm/s.

Plate I. Annual mean surface (0-45 m) velocity field. All vectors are shown. Unit vector=20 cm/s.

Plate II. Annual mean Atlantic layer (180-440 m) vector velocity field. All vectors are shown. Unit vector=10 cm/s.

Plate III. Annual mean intermediate layer (1100-1700 m) vector velocity field. All vectors are shown. Unit vector=5 cm/s.

FERRET Ver. 3.12
NOAA/PMEL TMAP
Jul 7 1995 17:04:11

DATA SET: moddepth.asc

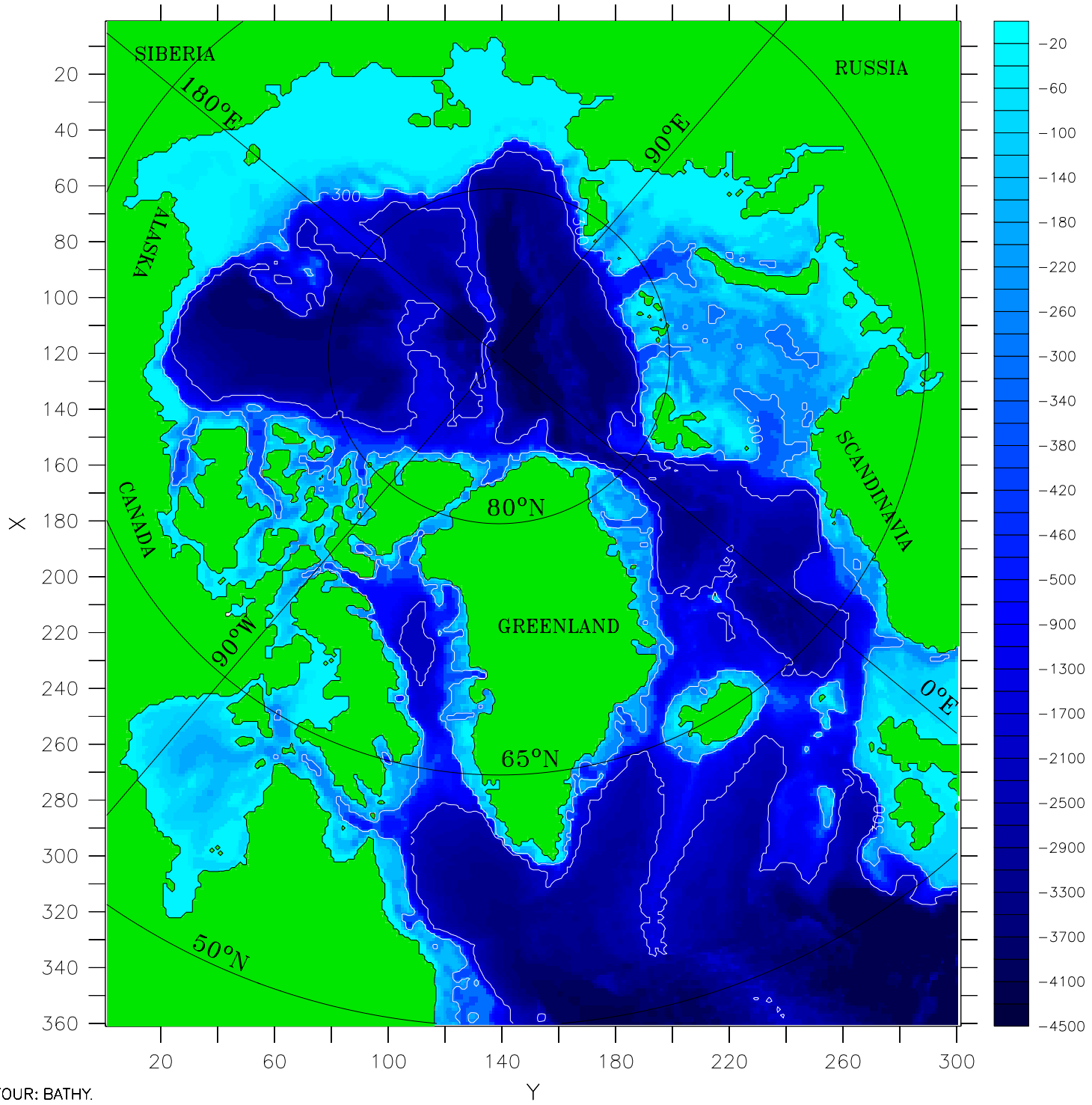

CONTOUR: BATHY.

Arctic Model Domain

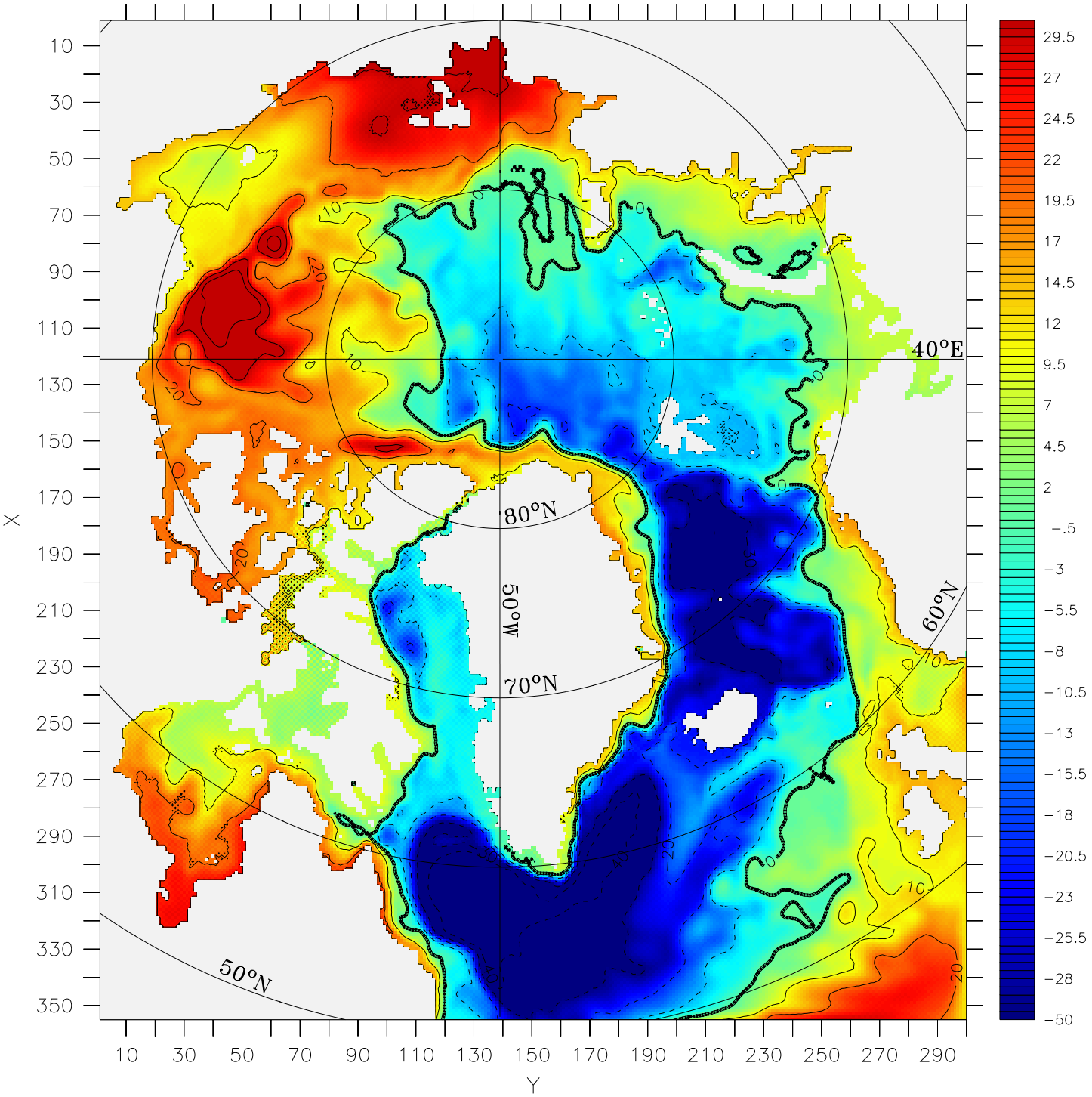

1992 Annual Mean Sea Level Height (cm)

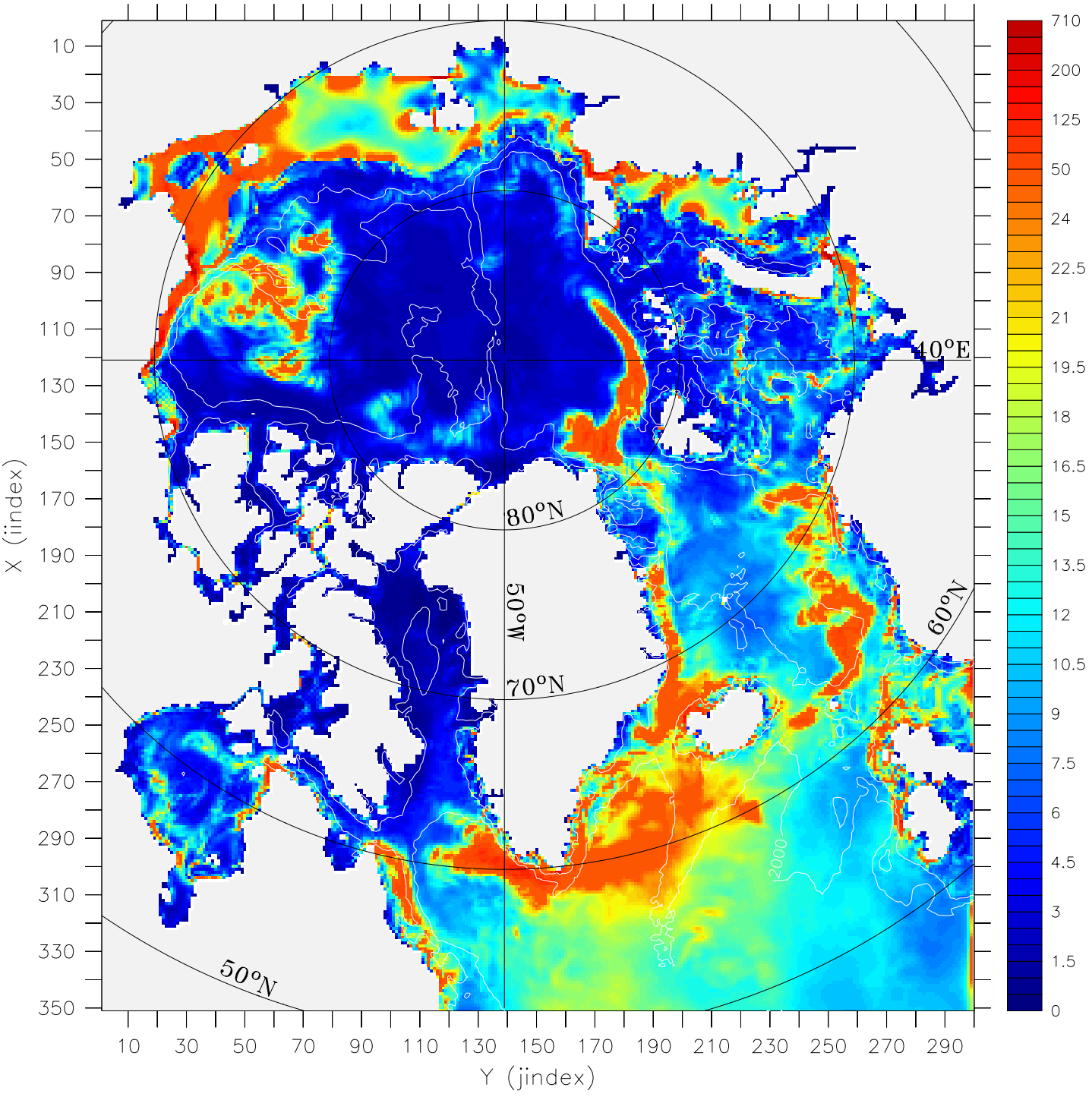

1992 Mean Surface Eddy Kinetic Energy (cm^2/s^2)

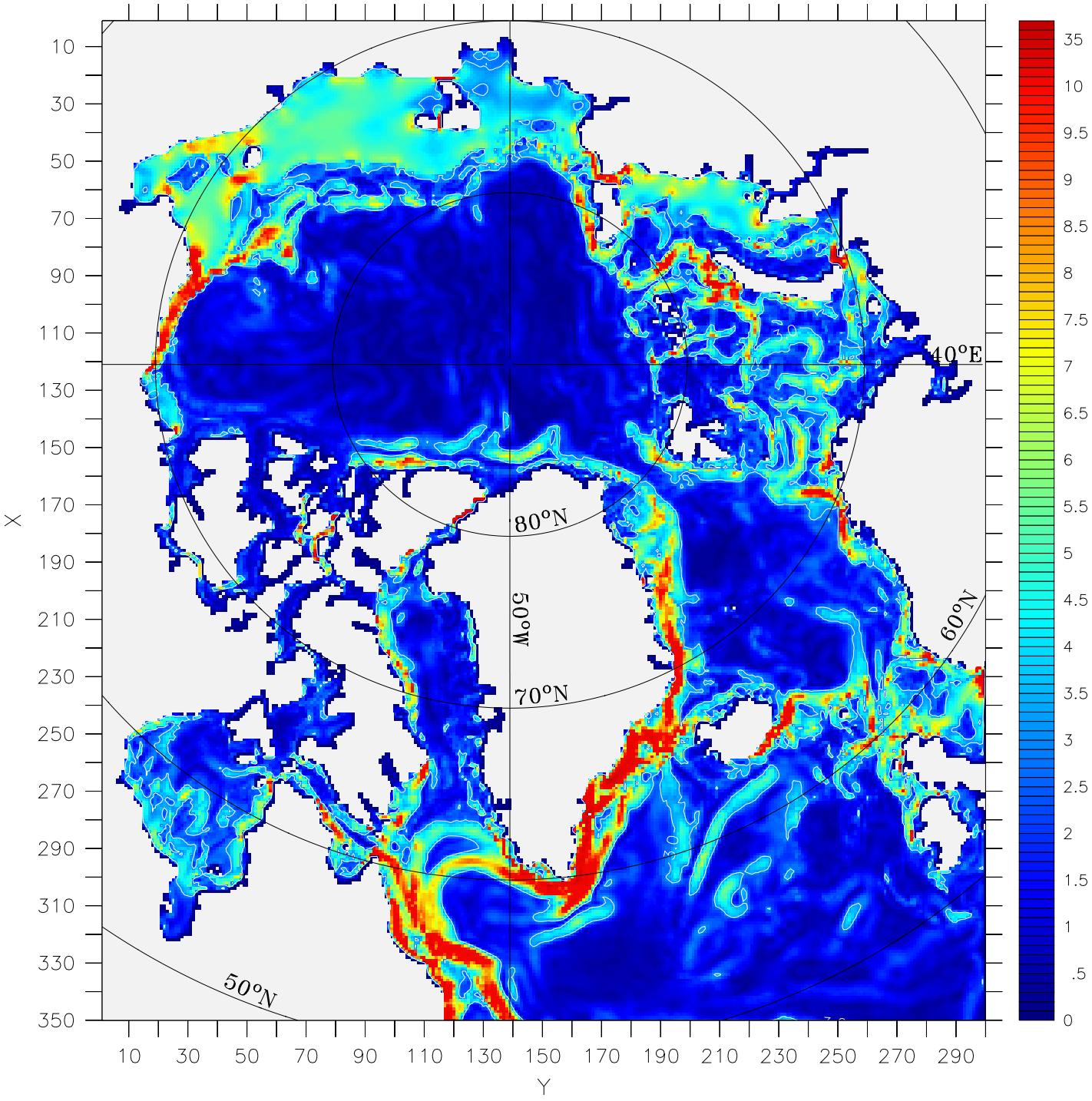

1992 Annual Mean Barotropic Velocity (cm/s), integration year=6,
white contour line shows 3 cm/s velocity.

FERRET Ver. 3.10
NOAA/PMEL TMAP
Mar 4 1995 00:04:04

TIME : 06-DEC-1993 00:00

DATA SET: tvel_3.72

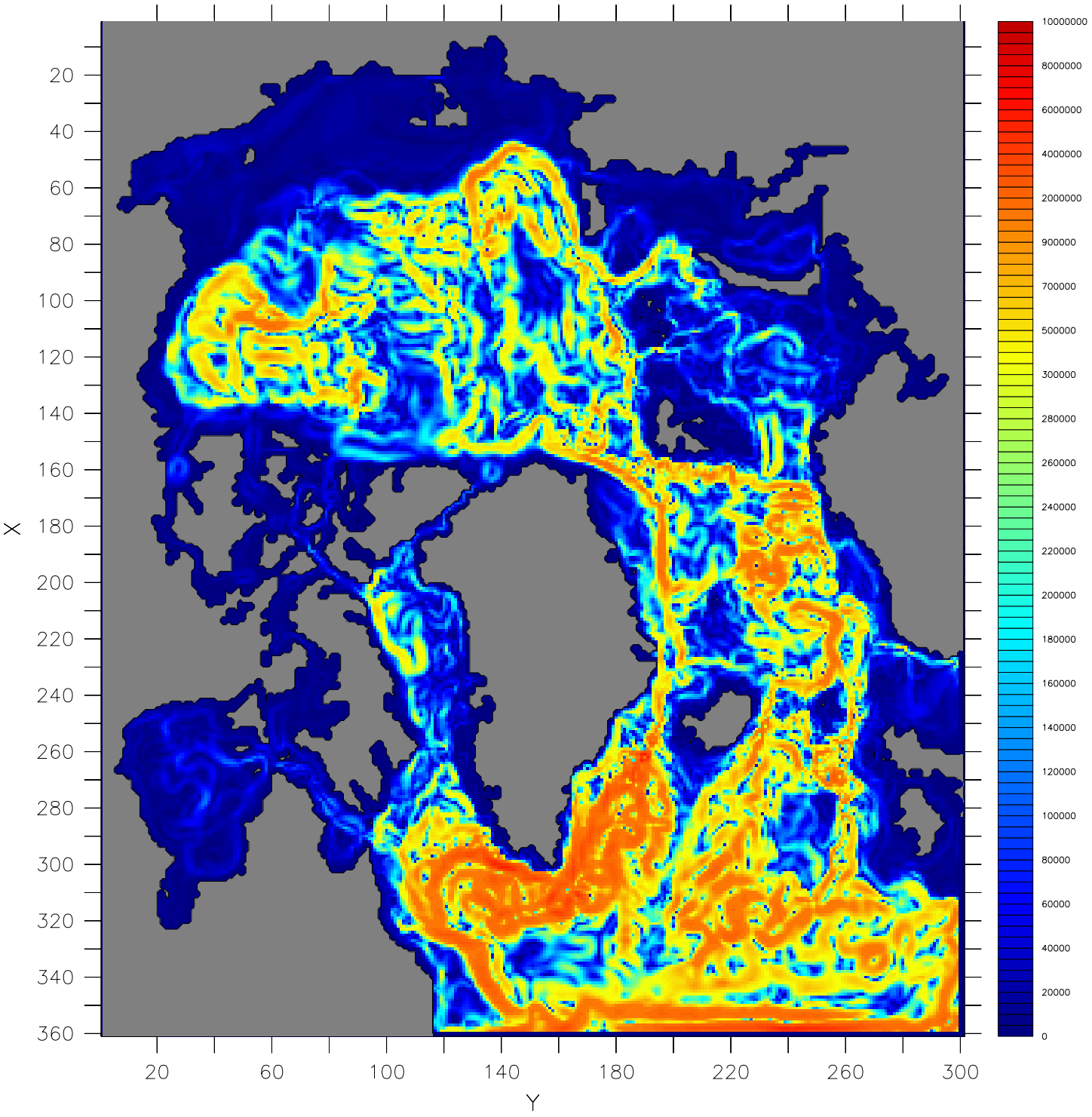

Mass transport/unit width (cm2/sec)

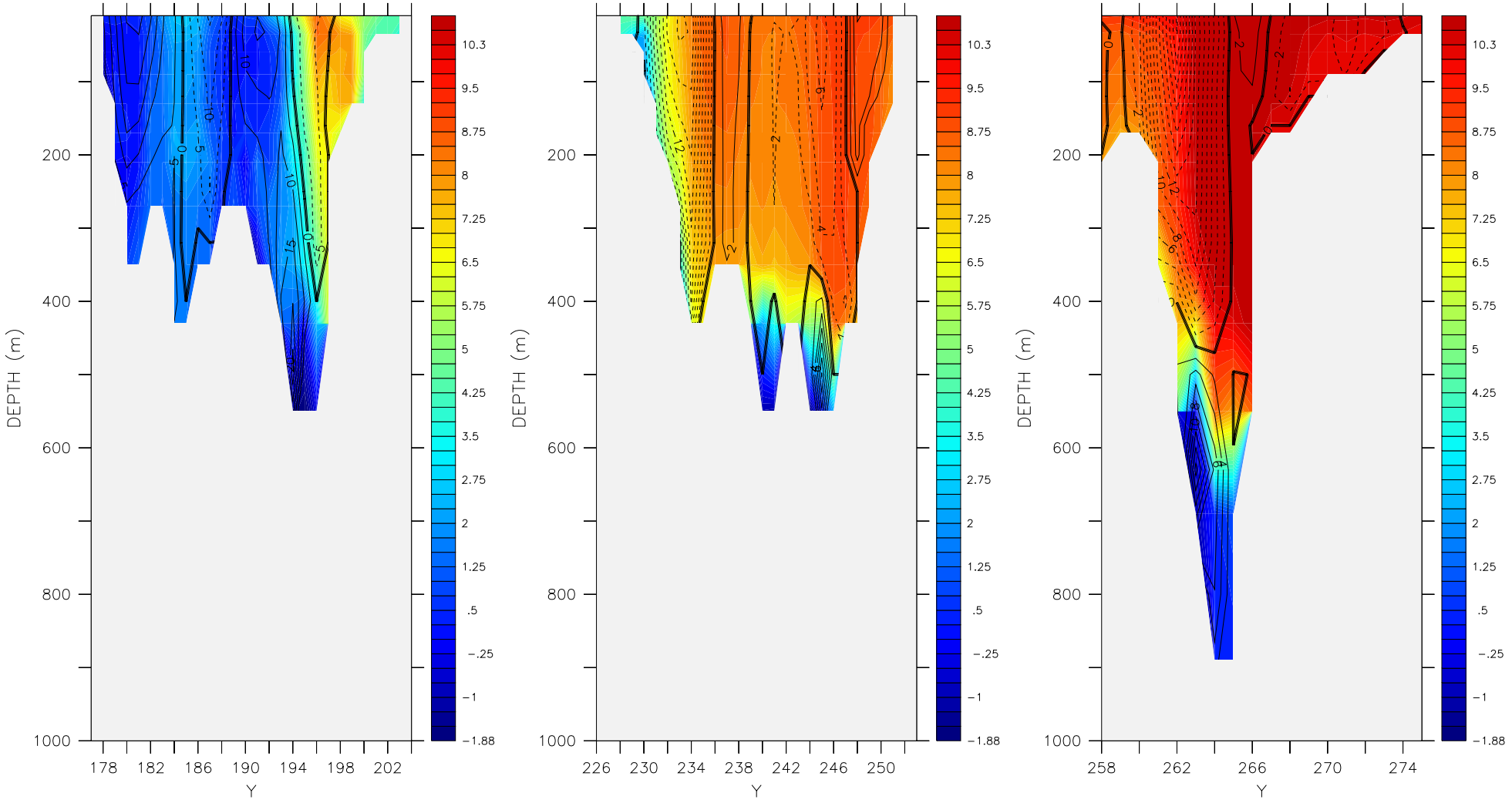

Annual Mean T&U (positive southward, cm/s) Section: Greenland–Iceland–Scotland Ridge.

Left: Denmark Strait (x=252), middle: Iceland–Faroe (x=243), right: Faroe–Shetland (x=245).

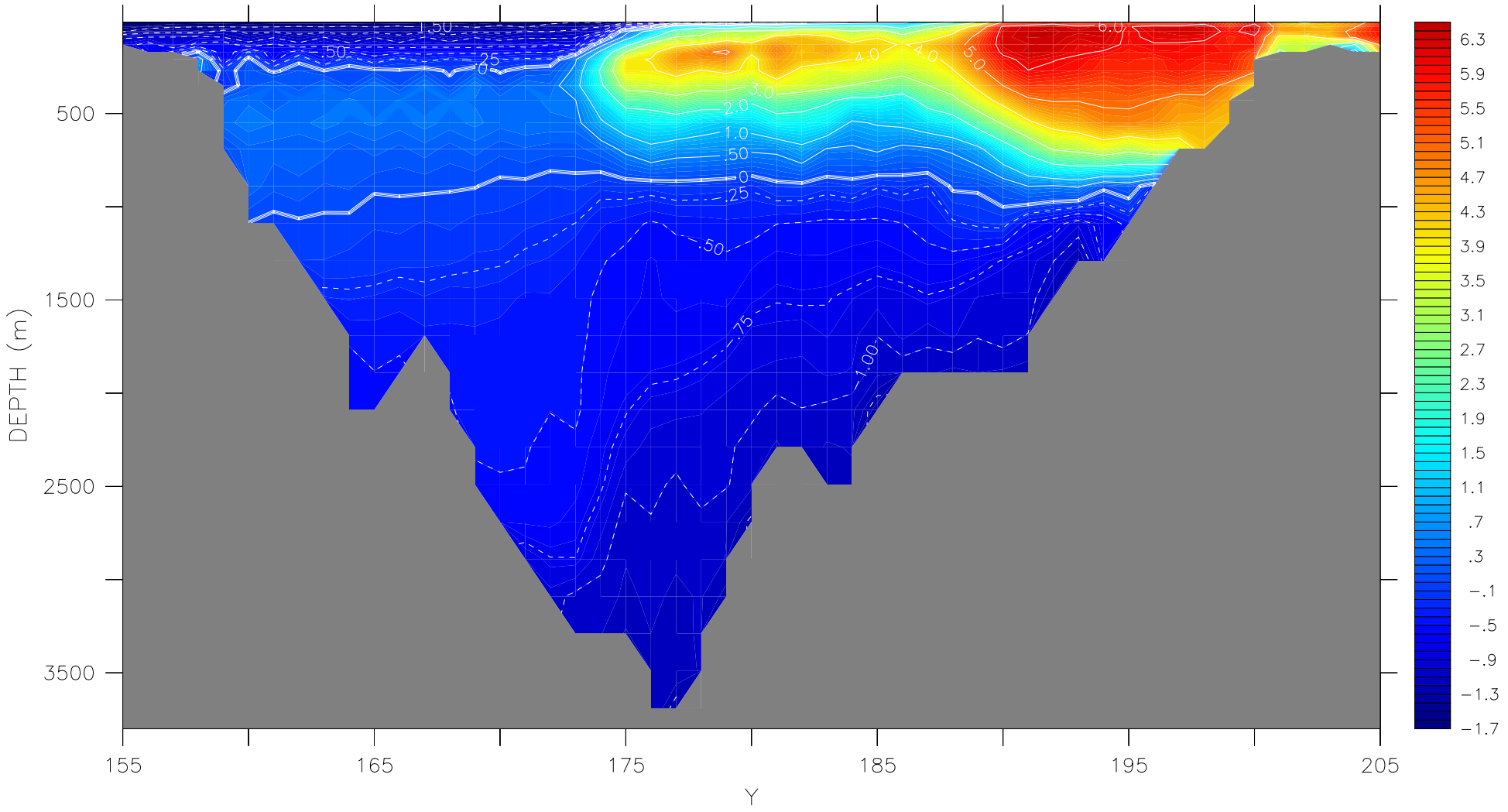

Fram Strait Annual Mean Temperature Section (°C) (year=6; x=156

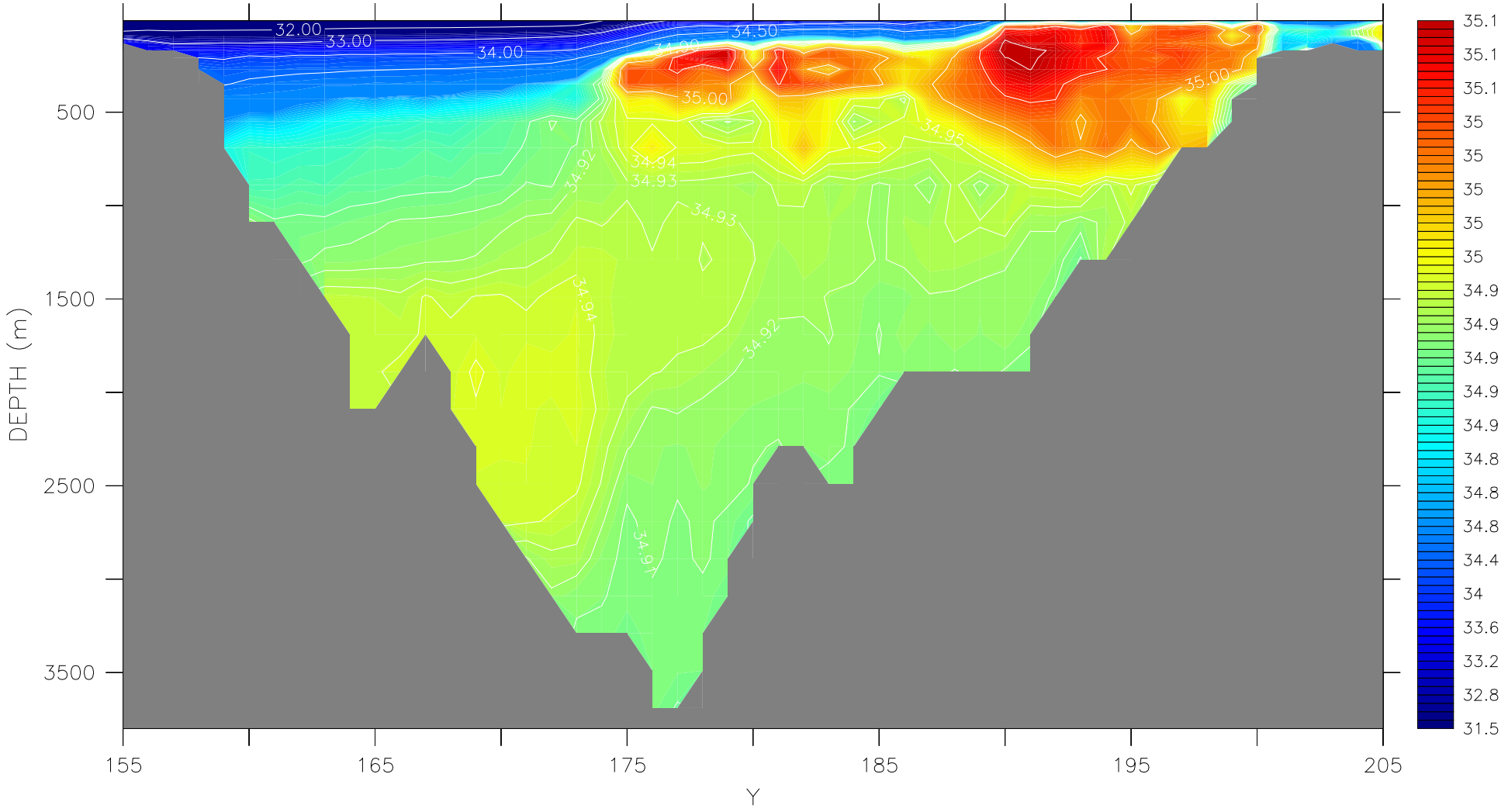

Fram Strait Annual Mean Salinity Section (ppt) (year=6; x=15

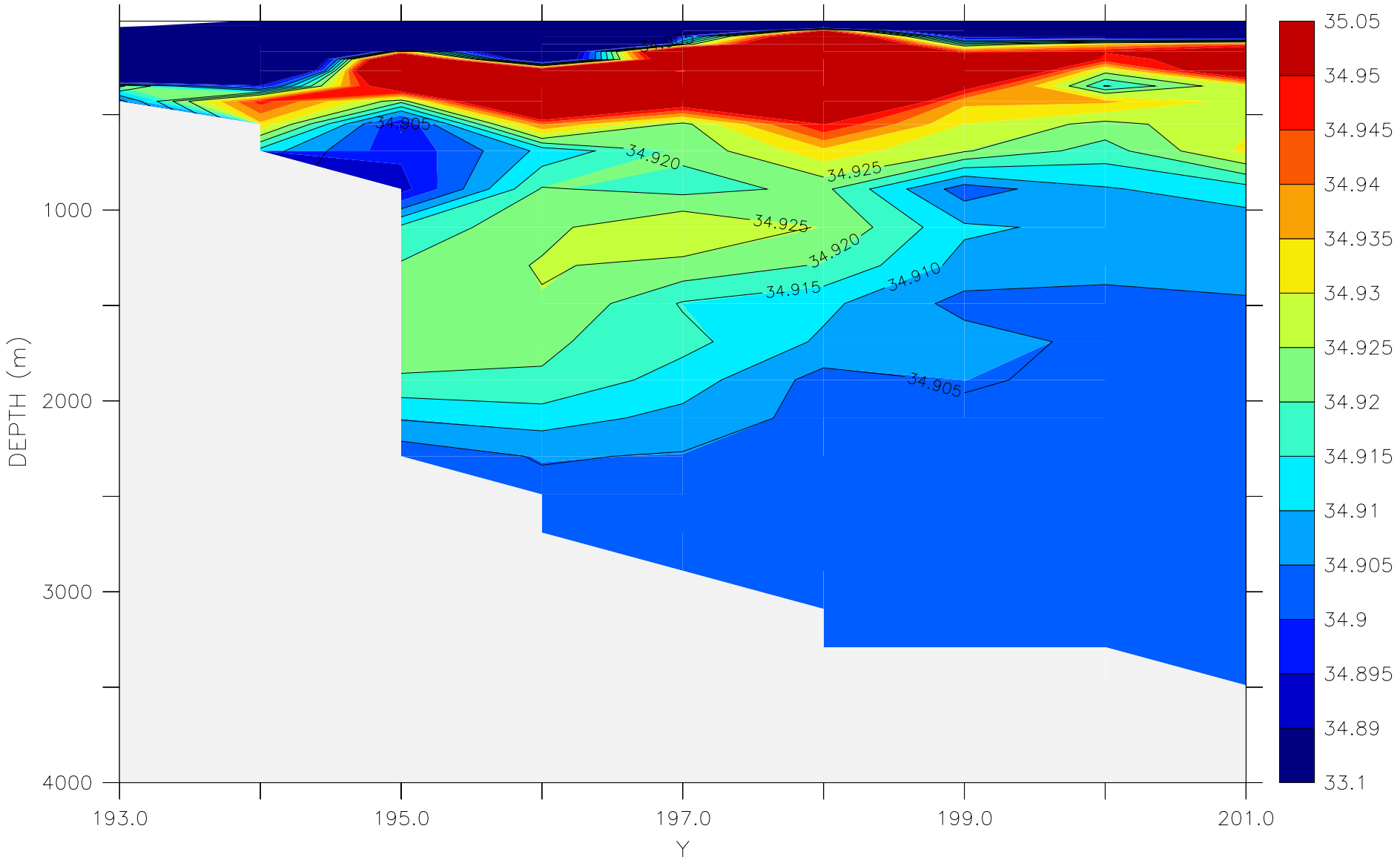

June 1992 Mean Salinity (ppt) Section (x=187): East Greenland Current.

FERRET Ver. 3.12
NOAA/PMEL TMAP
Dec 11 1996 21:59:30

LATITUDE : 74.5N

DATA SET: ocean_atlas_annual

World Ocean Atlas 1994 * 1x1 Degree Annual Means

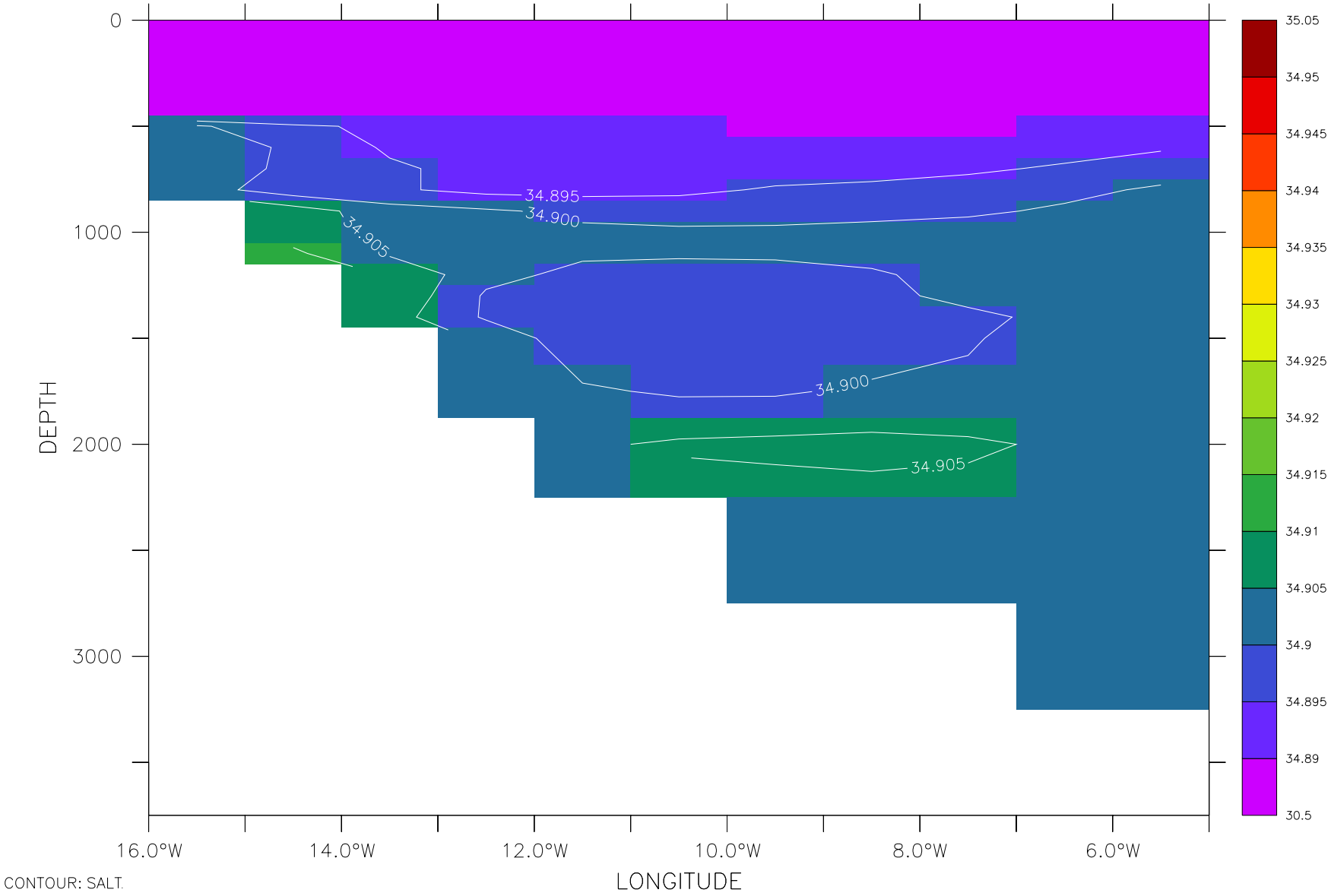

CONTOUR: SALT.

Salinity (psu)(From SAL00)

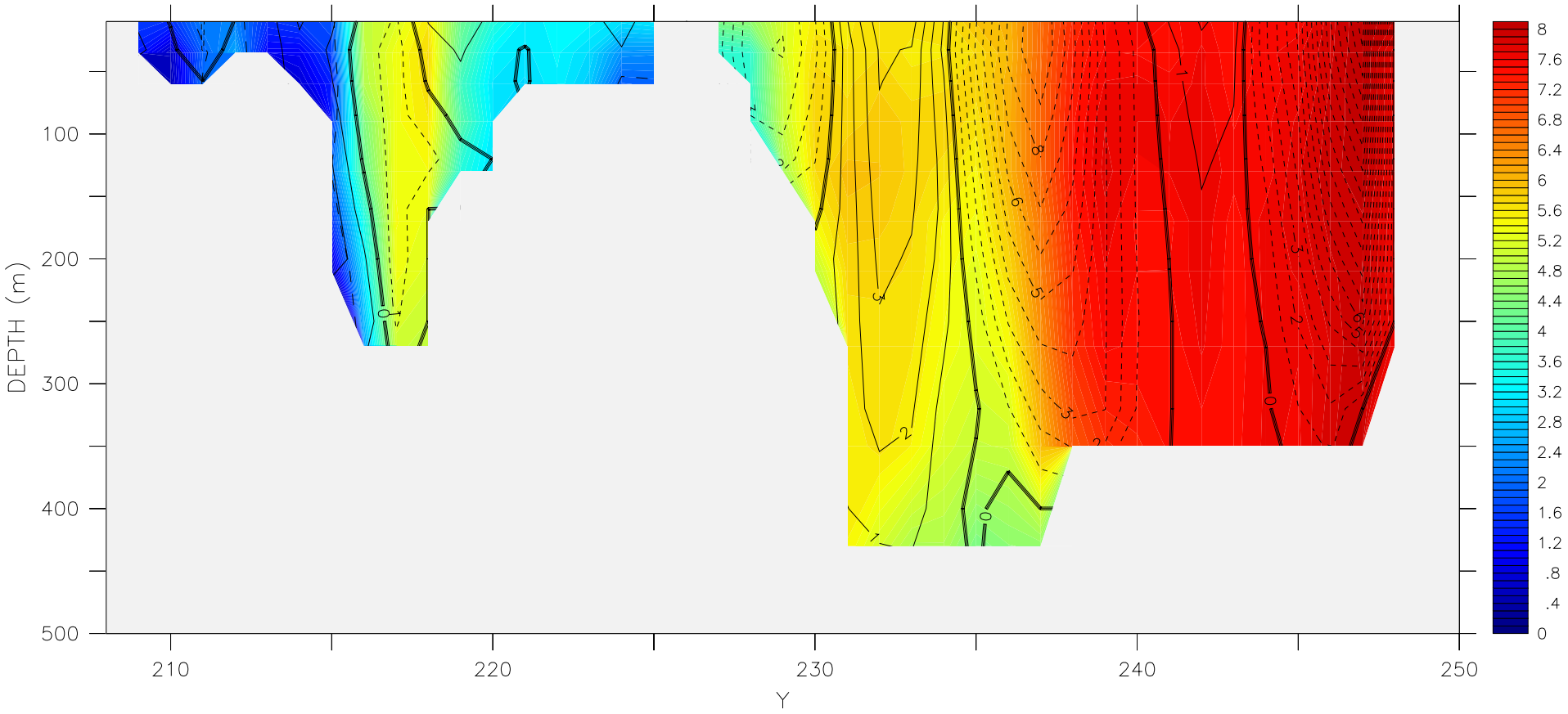

Annual Mean T&U (negative east, cm/s) Sec1(x=154): Norway–Bear Is.–Spitsbergen.

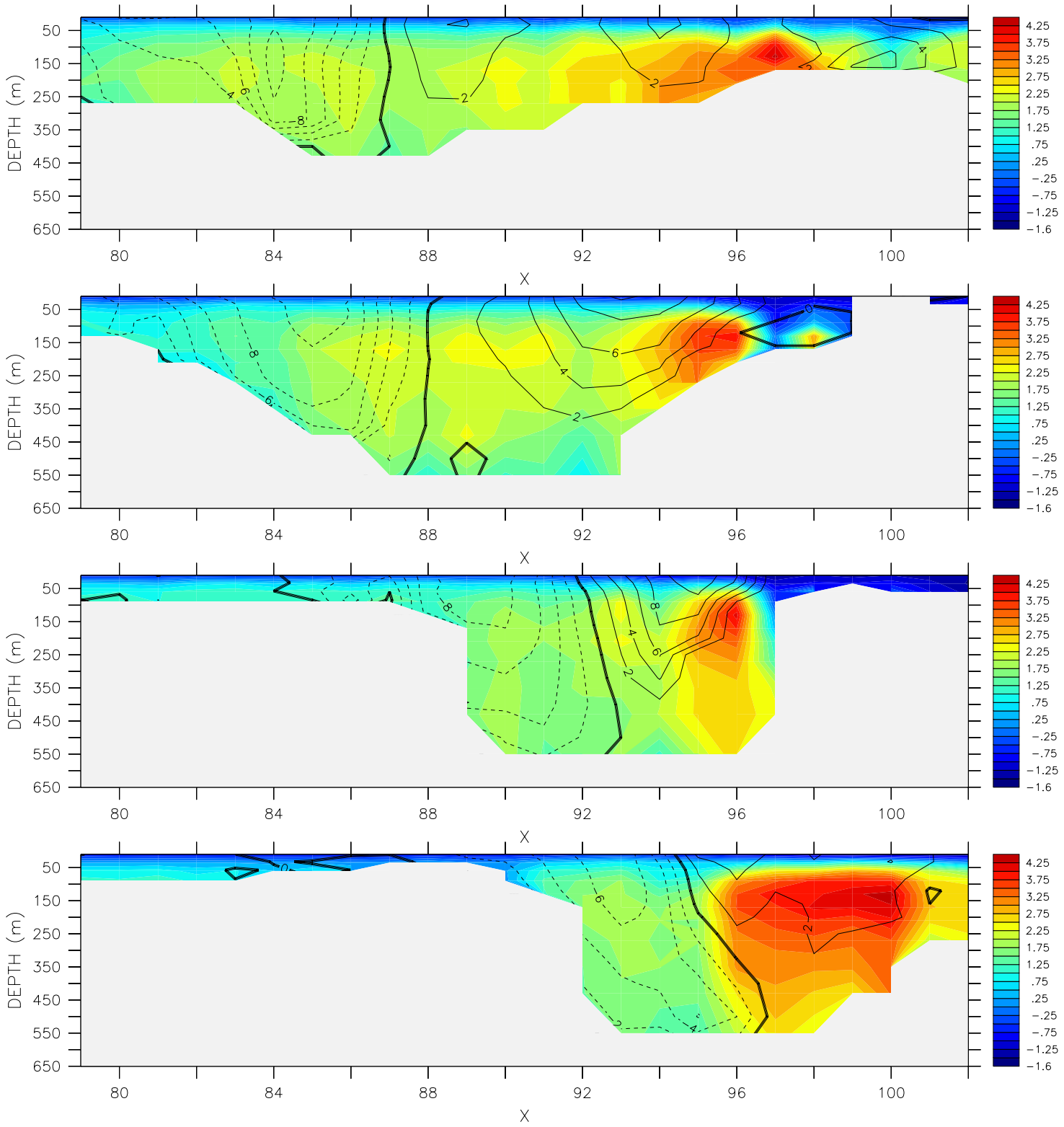

1992 Annual Mean St. Anna Through Temperature (°C) and Velocity (cm/s, positive south) Sections at y=201 (top), 193, 188, and 183 (bottom). Contour Intervals: 0.25°C and 2cm/s.

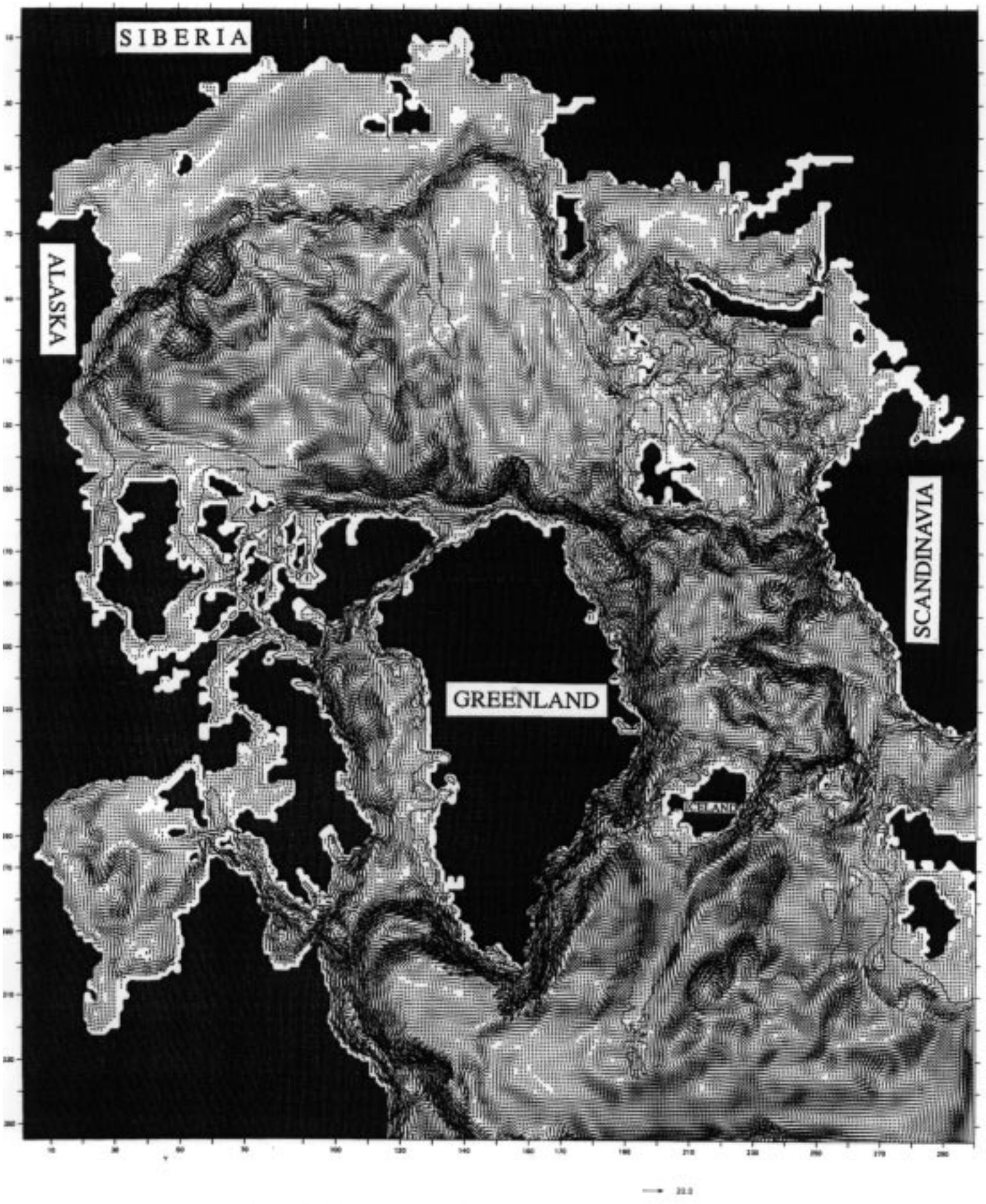

Annual Mean (1992) Surface (0-45m) Velocity (cm/s)

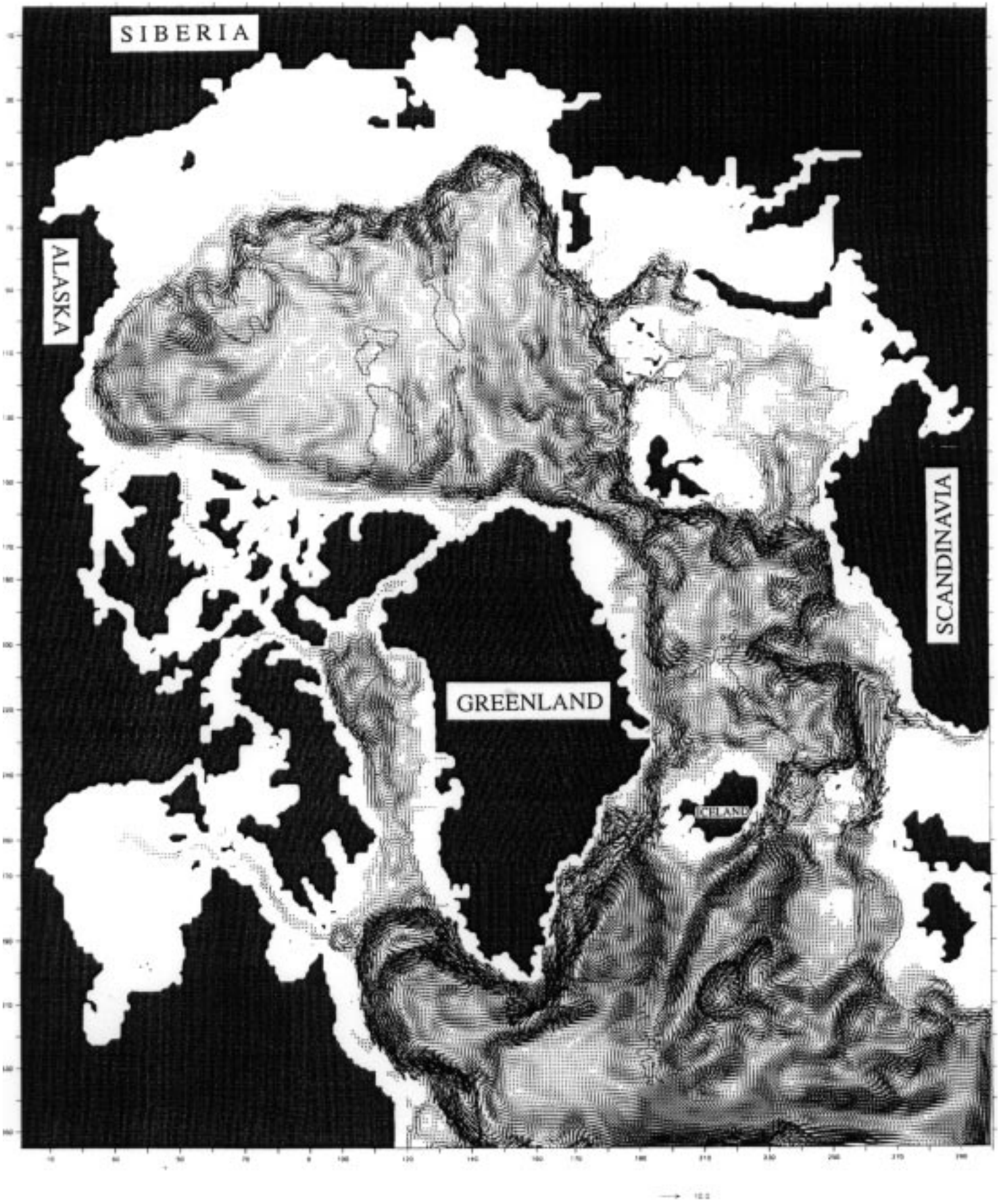

Annual Mean (1992) Atlantic Layer (180-440m) Velocity (cm/s)

Annual Mean (1992) Intermediate Layer (1100-1700m) Velocity (cm/s)